

BNWL-1125
UC-80



AEROSOL TRANSPORT
IN A CONDENSING-STEAM BOUNDARY LAYER

June 1, 1970



AEC RESEARCH &
DEVELOPMENT REPORT

BNWL-1125

LEGAL NOTICE

This report was prepared as an account of Government sponsored work. Neither the United States, nor the Commission, nor any person acting on behalf of the Commission:

A. Makes any warranty or representation, expressed or implied, with respect to the accuracy, completeness, or usefulness of the information contained in this report, or that the use of any information, apparatus, method, or process disclosed in this report may not infringe privately owned rights; or

B. Assumes any liabilities with respect to the use of, or for damages resulting from the use of any information, apparatus, method, or process disclosed in this report.

As used in the above, "person acting on behalf of the Commission" includes any employee or contractor of the Commission, or employee of such contractor, to the extent that such employee or contractor of the Commission, or employee of such contractor prepares, disseminates, or provides access to, any information pursuant to his employment or contract with the Commission, or his employment with such contractor.

PACIFIC NORTHWEST LABORATORY

RICHLAND, WASHINGTON

operated by

BATTELLE MEMORIAL INSTITUTE

for the

UNITED STATES ATOMIC ENERGY COMMISSION UNDER CONTRACT AT(45-1)-1830

3 3679 00061 4430

BNWL-1125

UC-80
Peactor Technology

AEROSOL TRANSPORT IN A CONDENSING-STEAM BOUNDARY LAYER

J.M. Hales
T.W. Horst
L.C. Schwendiman

Air Pollution Chemistry Section
and
Atmospheric Physics Section
of the
Atmospheric Resources Department
ENVIRONMENTAL & LIFE SCIENCES DIVISION

June 1, 1970

FIRST UNRESTRICTED
DISTRIBUTION MADE

AUG 12 '70

BATTELLE MEMORIAL INSTITUTE
Pacific Northwest Laboratories
Richland, Washington
99352

Printed in the United States of America
Available from
Clearinghouse for Federal Scientific and Technical Information
National Bureau of Standards, U.S. Department of Commerce
Price: Printed Copy \$3.00; Microfiche \$0.65

ABSTRACT

This report presents the results of a theoretical investigation of aerosol transport in a laminar, naturally convected, condensing-steam boundary layer. The boundary-layer equations given in previous literature have been extended to account for aerosol transport, and solved for various cases of interest using a hybrid-computer technique. Effects of diffusiophoresis, thermophoresis, and Brownian motion are included in the aerosol-transport analysis. Solutions are presented as profiles of temperature, velocity, steam concentration, and aerosol concentration. These are employed to obtain corresponding heat-transfer, aerosol-deposition, and condensation rates.

For very small particle sizes, aerosol-deposition rates were found to decrease with increasing particle size. For larger sizes, however, deposition rates were found to be independent of particle size, and subject only to conditions within the air-steam boundary layer. Computed deposition rates were compared with rates estimated by assuming particles to be deposited with the mass-average velocity of the air-steam mixture. Deposition rates estimated in this manner ranged from about 60% to 20% below those computed via the boundary layer model, depending on physical conditions of the system.

Steam condensation rates computed from the boundary-layer equations were compared with those estimated from experimental heat-transfer data on the basis of a heat-transfer - mass-transfer analogy. This comparison showed the analogy to be quite accurate over the range of conditions studied.

The computed results are discussed primarily in the context of nuclear reactor containment-vessel analysis, where the deposition of aerosols in condensing steam environments is of particular interest. These results, pertaining to laminar boundary layers only, are insufficient for a total description of containment-vessel behavior, where turbulence as well as a variety of engineered safeguard measures may be present. The definitive analysis of aerosol transport in laminar boundary layers presented here is an essential first step toward understanding of total system behavior. It is expected that a large portion of the value of this work will be realized in its subsequent application for future analyses of engineered safeguard measures and turbulent boundary layers.

TABLE OF CONTENTS

	<u>Page</u>
INTRODUCTION	1
OBJECTIVES	2
CHARACTERIZATION OF NATURALLY-CONVECTED, CONDENSING-STEAM BOUNDARY LAYERS	3
FORMULATION OF GOVERNING EQUATIONS	7
FORMULATION OF BOUNDARY CONDITIONS	10
SIMILARITY TRANSFORMATION	11
WALL-FLUX EQUATIONS	15
ESTIMATION OF PHYSICAL PROPERTIES	16
SOLUTION OF BOUNDARY-LAYER EQUATIONS	16
RESULTS	19
<u>Solutions of Steam, Energy, and Momentum Transport Equations</u>	19
<u>Solutions of Particle-Transport Equation</u>	19
<u>Wall-Transport Calculation</u>	25
<u>Humidity in the Boundary-Layer Region</u>	25
<u>Particle Trajectories</u>	25
DISCUSSION OF RESULTS	30
<u>Validity of Equations</u>	30
<u>Accuracy of Computations</u>	33
<u>Simplified Analysis of Heat and Vapor Transport -- Test of</u> <u>Heat Transfer-Mass Transfer Analogy</u>	34
<u>Simplified Analysis of Aerosol Transport</u>	36
<u>Relative Contributions to Particle Transport by Individual</u> <u>Mechanisms</u>	37
APPLICATION TO REAL SYSTEMS	40
REFERENCES	45
TABLE OF NOMENCLATURE	47
APPENDIX 1	49
APPENDIX 2	53
APPENDIX 3	57

AEROSOL TRANSPORT IN A CONDENSING-STEAM BOUNDARY LAYER

INTRODUCTION

In the unlikely event of a loss-of-coolant accident, reactor-core overheating may lead to fuel failure and the consequential release of steam and radioactive fission products to the containment vessel atmosphere. Because of potential hazards to the outside environment, it is imperative that these fission products be immobilized as rapidly as possible. It is important also to promote rapid condensation of steam within the system, thus suppressing pressure buildup and preventing overstressing of the containment structure.

Removal of steam and fission products may be augmented by engineered safeguard measures, which are designed to enhance the natural process of immobilization. Such measures often depend on common mechanisms of removal. Information pertaining to each of these mechanisms, therefore, should be useful for analysis of a variety of safeguard measures. The present investigation is concerned primarily with removal through natural transport to the containment vessel walls; however, the insights provided concerning the nature of such basic mechanisms as diffusiophoresis, thermophoresis, and particle diffusion should be beneficial to other studies where engineered safeguards are analyzed in closer detail.

Past experiments have demonstrated that wall-transport processes associated with post-accident containment system environments give rise to a characteristic boundary-layer structure. The understanding of transport across such boundary layers is adequate for most situations involving laminar flow in the absence of aerosol. This understanding is incomplete, however, for conditions wherein turbulence and/or the deposition of aerosol occurs.

Boundary-layer phenomena associated with heat and vapor transport in laminar, naturally-convected, condensing systems have been investigated previously on rigorous theoretical bases. [10,11,13,15,16] Similar attempts for turbulent boundary-layers have been more restricted, and have met with little success. [3,4,8] To our knowledge, there is essentially no published work concerning aerosol interactions in either turbulent or laminar boundary layers of this type.

In view of this present state of theoretical development, it is appropriate to direct further investigation toward understanding aerosol behavior

in laminar, condensing-steam boundary layers. It is expected that laminar boundary layers will exist to some extent in all post-accident systems. In addition, a thorough investigation of laminar deposition processes will provide substantial insight for further analyses to be made of the turbulent regime. Finally, detailed (although idealized) information concerning particle transport in laminar boundary layers will be helpful in explaining phenomena occurring in connection with engineered safeguard measures.

A thorough investigation of particle transport in laminar boundary layers should attempt to answer the following questions:

1. Under what conditions do laminar and turbulent boundary layers exist?
2. What interrelations exist between the processes for momentum, energy, steam, and particle transport, and what are the physical characteristics of laminar boundary layers?
3. What paths, i.e., trajectories, do the aerosol particles follow during the deposition process?
4. How adequately can the deposition process be represented mathematically?
5. Can simpler, semi-empirical correlations and analogies be used to predict transport rates, rather than the more complex boundary-layer analysis?
6. How can results of the boundary-layer analysis be applied to real systems?

OBJECTIVES

The primary objective of this investigation is to consider each of the foregoing questions on the basis of a theoretical analysis of boundary layer behavior. Qualitative aspects of such behavior are discussed in the following section. Subsequent sections will deal with development of quantitative equations, their solution, and their application to real physical systems.

CHARACTERIZATION OF NATURALLY-CONVECTED, CONDENSING-STEAM
BOUNDARY LAYERS

The mathematical modeling presented in this paper will be focused upon condensing-steam boundary layers that are formed adjacent to a semi-infinite, vertical, flat plate. Use of this idealization is expedient because of mathematical tractability and because of similar assumptions employed in previous theoretical work. Practical consequences of the vertical-plate assumption will be discussed in a later section.

Boundary layers occurring under such circumstances are typified by the drawing shown in Figure 1. Here the boundary layer initiates at the plate top, the gases in the vicinity of the face being accelerated downward by virtue of their increased density. For condensing steam-air mixtures, the density gradient in the wall region occurs as a consequence of gradients in both temperature and concentration. The laminar boundary layer grows continuously with distance down the plate. Such growth is manifested in both the thickness of the boundary layer and in increased flow in the vertical direction. At some distance from the top of the wall, the laminar regime gives way to a transition to turbulent flow. Once fully-developed, the turbulent boundary layer is not expected to change significantly with increasing distance down the wall.

The material required for growth of the laminar boundary layer is supplied by an influx of bulk gas as shown in Figure 1. A portion of the steam in this gas mixture migrates to the interface and condenses; the remainder is accelerated in the downward direction. Since downward acceleration is small for the case of a turbulent boundary layer, the corresponding influx is of lesser magnitude, as indicated by the schematic.

Conditions for the existence of a stable, laminar boundary layer can be estimated from known behavior of noncondensing systems. Intuitively, one should expect the conditions to depend primarily upon the Grashoff number (Gr , ratio of buoyancy to viscous forces). These conditions should depend also on the Prandtl (Pr) and Schmidt (Sc) numbers (which influence the boundary layer widths), although these dependences should be of only secondary importance. Pr and Sc are comparable in magnitude, and do not vary appreciably for air-steam mixtures; hence it is allowable to express conditions for the flow regimes in terms of Gr only.

From data obtained from noncondensing fluids^[15], the following condition

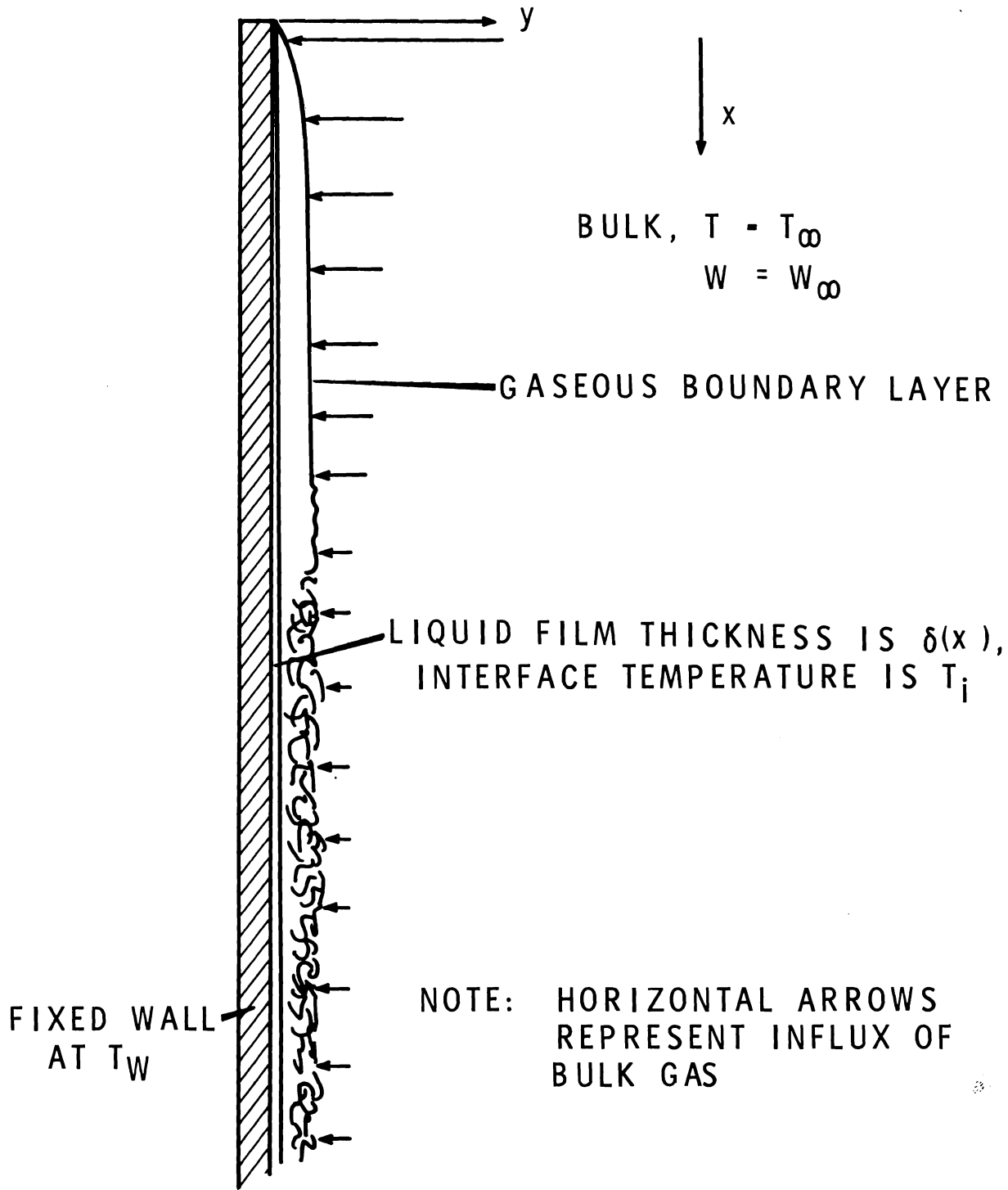


FIGURE 1

SCHMATIC OF BOUNDARY LAYER FORMATION
ADJACENT TO A VERTICAL WALL

may be written,

$$\text{laminar} \leftarrow 1.5 \times 10^8 < \overset{\text{transitional}}{\text{Gr}} > 1.5 \times 10^{10} \rightarrow \text{turbulent.} \quad (1)$$

Gr may be expressed (taking advantage of the ideal-gas law), as

$$\text{Gr} = \frac{gL^3}{\nu^2} \left[\frac{(M_a - M_w)(x_{wi} - x_{w\infty})}{(M_a - M_w)x_{w\infty} - M_a} + \frac{T_\infty - T_i}{T} \right]. \quad (2)$$

Here M represents molecular weight, x_w represents mole fraction of water, and the distance down the wall is given by L. The first term in brackets relates to buoyancy arising as a consequence of the concentration gradient across the boundary layer; the second term reflects buoyancy changes owing to the associated temperature gradient.

Figure 2 shows solutions of equation (2) for a set of conditions in the range of interest to the present investigation. From this figure it is seen that the transition zone is expected to cover a relatively wide range of conditions. The laminar boundary layer will be confined to several feet from the top of the vertical condensation surface, and depend upon the temperature difference between the wall and the bulk gas.

Liquid condensate will be influenced by gravity also, and will run down the wall surface as a result. Ideally, such runoff will conform to laminar-film behavior; however, such nonideal factors as liquid ripples and drop-wise condensation are often encountered in practice. Presence of condensate adds a further barrier to heat transfer, since it acts as an insulating surface; it also serves to alter the velocity profile of the gaseous boundary layer, owing to its own x-component of velocity.

Aerosol particles in the system are influenced by a number of phenomena. Particle velocity is known to be a rather complex function of the effects of Brownian motion, thermal diffusion, diffusiophoresis, bulk convection effects, and gravity. Owing to this dependence, particle transport is seen to be quite intimately related to other boundary-layer phenomena. For systems involving relatively dilute suspensions of small particles, all gravitational effects associated with the particles may be neglected. In addition, several other simplifying assumptions can be justified. These will be considered in detail in the following section of this report.

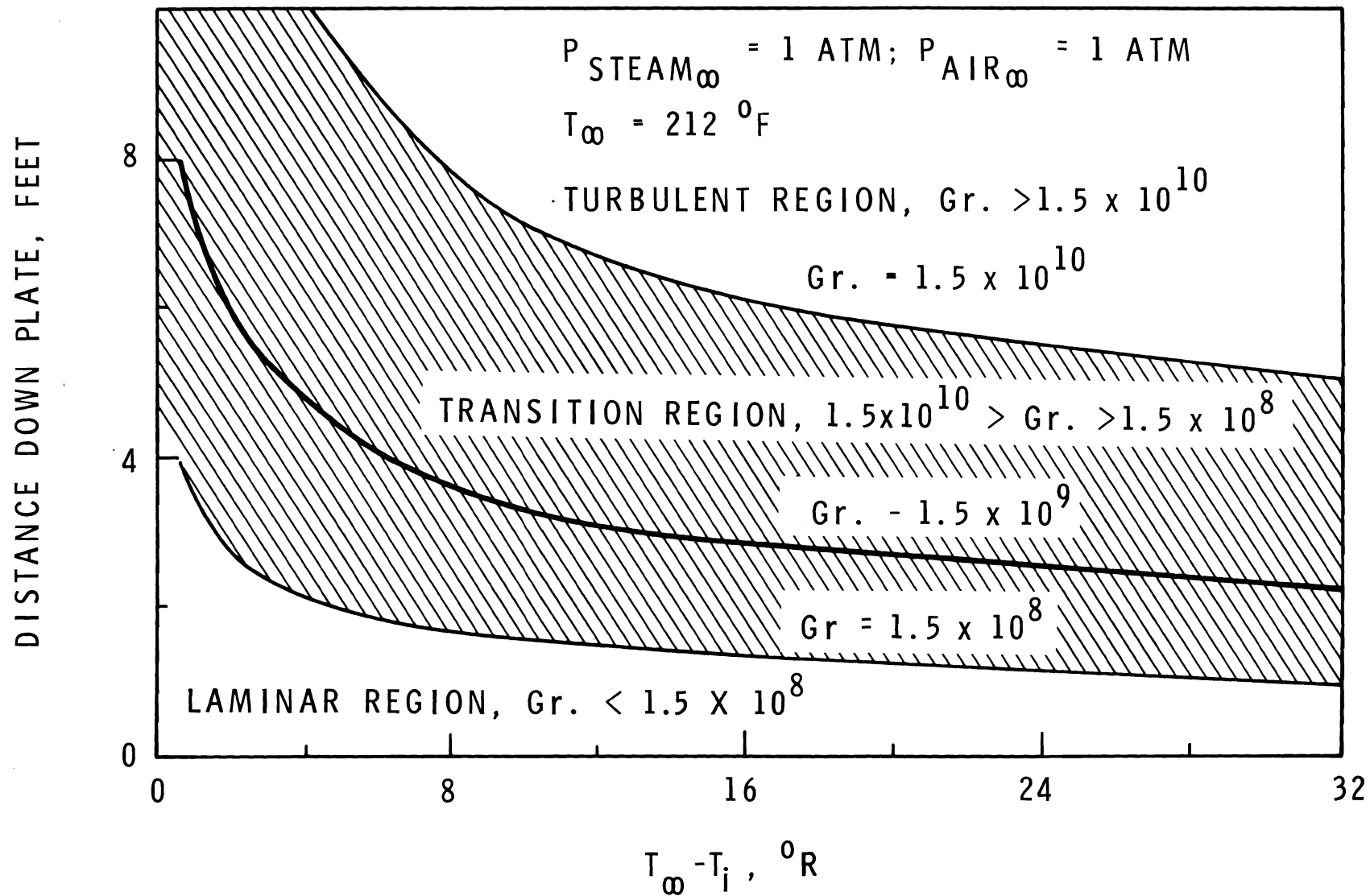


FIGURE 2

EXPECTED POINTS OF TRANSITION FROM LAMINAR TO
TURBULENT BOUNDARY LAYER

FORMULATION OF GOVERNING EQUATIONS

Figure 1 gives the basis for formulation of the boundary-layer equations. A bulk mixture of steam, air and aerosol is exposed to the condensation surface, which is maintained at the temperature T_w . Steam from the bulk mixture migrates to the wall, forming a liquid film which runs off under the force of gravity. The convention will be used that energy, gas, and aerosol fluxes away from the wall are positive entities.

Presence of the liquid film in addition to the gaseous boundary layer causes heat transfer to occur as a two-step process. By making some reasonable assumptions one can reduce the complexity of the mathematics associated with this process, allowing solutions for each step to be obtained individually. Once formulated, these solutions can be matched at the interface, giving a composite description of the total system.

Heat transfer through a liquid film formed upon condensation of a pure vapor has been treated in a satisfactory manner by Nusselt.^[12] Nusselt's derivation may be extended to situations wherein a noncondensable gas is present, provided that the gas-liquid interface temperature, T_i , is independent of position. Assumption of constant T_i is allowable whenever the temperature drop across the liquid film is small compared to that across the gaseous boundary-layer -- a condition that is met for almost all practical situations.^[6]

Use of Nusselt's derivation implies acceptance of all assumptions employed therein. The validity of these assumptions has been discussed at length elsewhere.^[11] The most important of them are listed as follows:

1. Zero shear at the gas-liquid interface.
2. Constant liquid properties (except temperature).
3. Zero viscous dissipation.
4. Constant energy flux across liquid film.

Description of the gaseous boundary layer is accomplished using the appropriate forms of the equations for conservation of mass, momentum, and energy.^[1] Assuming zero viscous dissipation, zero longitudinal diffusion, and negligible coupled transport effects such as thermal diffusion and diffusion thermo, Minkowycz and Sparrow^[11] have listed these equations for the situation wherein aerosol is absent. These equations are valid for aerosol-containing systems, provided the presence of aerosol does not significantly affect the bulk properties of the gas. The equations are listed as follows:

TOTAL MASS:

$$\frac{\partial}{\partial x} (\rho u) + \frac{\partial}{\partial y} (\rho v) = 0, \quad (3)$$

MASS OF WATER:

$$\rho u \frac{\partial W}{\partial x} + \rho v \frac{\partial W}{\partial y} = \frac{\partial}{\partial y} (\rho D_{AB} \frac{\partial W}{\partial y}), \quad (4)$$

MOMENTUM:

$$\rho u \frac{\partial u}{\partial x} + \rho v \frac{\partial u}{\partial y} = g(\rho - \rho_\infty) + \frac{\partial}{\partial y} (\mu \frac{\partial u}{\partial y}), \quad (5)$$

and ENERGY:

$$\rho C_p u \frac{\partial T}{\partial x} + \rho C_p v \frac{\partial T}{\partial y} + (C_{pa} - C_{pw}) \rho D_{AB} \frac{\partial W}{\partial y} \frac{\partial T}{\partial y} = \frac{\partial}{\partial y} (k \frac{\partial T}{\partial y}). \quad (6)$$

The nomenclature used in equations (3) through (6) is consistent with that found in most published treatments of this subject, and a complete definition of the symbols is given in the Table of Nomenclature. However, it should be noted that here W denotes the mass fraction of water. This contrasts to the W of Minkowycz and Sparrow, which denotes the mass fraction of air.

For a complete description of aerosol-containing systems an additional equation is required. This accounts for conservation of the aerosol species, and may be written as follows:

$$\frac{\partial N v_p}{\partial y} + \frac{\partial N u_p}{\partial x} = 0, \quad (7)$$

where N is the number concentration of particles, and v_p and u_p are the mean particle velocities in the y and x directions, respectively. Equation (7) is valid for any aerosol under steady-state conditions, provided that no generation or decay occurs.

In view of the physical situation of interest, it is justifiable to let the x -component of the particle velocity equal the mass-average velocity in that direction, i.e.,

$$u_p = u. \quad (8)$$

Particles moving in the y-direction also are influenced by the bulk velocity. Here, however, correction terms arising from thermophoresis, counter-diffusion of air and water, and particle diffusion may become important. Assuming an additive relationship, the net effect of these contributions may be represented as

$$v_p = v + v_c + v_t - \frac{D}{N} \frac{\partial N}{\partial y}, \quad (9)$$

where D is the aerosol diffusion coefficient, giving the aerosol diffusion flux in terms of a mass-fixed frame of reference.

The diffusio-phoretic correction term, v_c , depends on the aerosol-particle size and its relation to the mean-free-path of the gas molecules. For conditions wherein the mean-free-path is large compared to particle size, (free-molecule regime), Waldmann^[17] has developed the following equation:*

$$v_c = - \frac{D_{AB}}{W + \frac{1}{\sqrt{\frac{M_a}{M_w} - 1}}} \frac{\partial W}{\partial y}. \quad (10)$$

Free-molecule conditions will be assumed throughout this study. Waldmann has also formulated an expression for the thermophoretic contribution to particle velocity. This may be expressed as:

$$v_t = - \frac{k}{5P} \frac{\partial T}{\partial y}, \quad (11)$$

where k is the thermal conductivity and P is total system pressure.

With these substitutions equation (7) becomes:

$$\frac{\partial(Nv)}{\partial y} + \frac{\partial(Nu)}{\partial x} - \frac{\partial}{\partial y} \left[\frac{N D_{AB}}{W + \frac{1}{\sqrt{\frac{M_a}{M_w} - 1}}} \frac{\partial W}{\partial y} \right] - \frac{\partial}{\partial y} \left[\frac{Nk}{5P} \frac{\partial T}{\partial y} \right] = \frac{\partial}{\partial y} \left[D \frac{\partial N}{\partial y} \right], \quad (12)$$

completing the formulation of conservation equations for the gaseous boundary layer.

* Equation (10) appears in a form somewhat different from that given by earlier authors. This is because of the necessity to express the correction in terms of the mass-average velocity, v , rather than the molar-average velocity which is used traditionally.

FORMULATION OF BOUNDARY CONDITIONS

The liquid-film description given by Nusselt can be conveniently matched to the foregoing system of equations through boundary-conditions at the gas-liquid interface. Neglecting interfacial resistance, one may write immediately,

$$T = T_i \text{ at } y = \delta, \quad (13)$$

and

$$W = W_i \text{ (saturation value at } T_i) \text{ at } y = \delta. \quad (14)$$

As a consequence of the absence of interfacial slip,

$$u_L = u_G \text{ at } y = \delta. \quad (15)$$

In terms of Nusselt's model this becomes,

$$u_G = \left[-\frac{q_t \delta \times \rho'}{\lambda \mu_L} \right]^{1/2} \text{ at } y = \delta, \quad (16)$$

where q_t is the total heat flux from the wall and λ is the latent heat of vaporization of water.

In addition, conservation of air and energy at the gas-liquid interface gives

$$\rho u \frac{d\delta}{dx} - \rho v = \frac{\rho D_{AB}}{1 - W_i} \frac{\partial W}{\partial y} \text{ at } y = \delta, \quad (17)$$

and

$$\frac{-\rho D_{AB}}{1 - W_i} \frac{\partial W}{\partial y} \lambda - k \frac{\partial T}{\partial y} = q_t \text{ at } y = \delta, \quad (18)$$

respectively.

Finally, a description of aerosol concentration at the interface is required. This is given simply by defining an interface concentration,

$$N = N_i \text{ at } y = \delta. \quad (19)$$

Boundary conditions at infinity depend on the assumption of a well-mixed bulk. These are largely self-explanatory, and are given as follows:

$$T = T_{\infty} \quad \text{at } y = \infty, \quad (20)$$

$$W = W_{\infty} \quad \text{at } y = \infty, \quad (21)$$

$$N = N_{\infty} \quad \text{at } y = \infty, \quad (22)$$

$$u = 0 \quad \text{at } y = \infty, \quad (23)$$

completing the description of boundary conditions for the gaseous boundary-layer model.

SIMILARITY TRANSFORMATION

Often, through an appropriate combination of variables, one can transform a set of partial differential equations into an equivalent set of ordinary differential equations. This reduction in the number of independent variables is usually accomplished at the expense of raising the order of the transformed equations. Such transformations serve to simplify the problem of solving the partial differential equations, and are known as similarity transformations.

Minkowycz and Sparrow^[11] have introduced a similarity transformation for the steam-air boundary-layer problem described in the preceding sections. In applying the transformation, these authors followed the conventional procedure of introducing a stream function, ψ , defined so as to satisfy the total continuity equation:

$$u = \pi \frac{\partial \psi}{\partial y}; \quad v = -\pi \frac{\partial \psi}{\partial x}. \quad (24a,b)$$

Here π is the density ratio, ρ_{∞}/ρ .

These authors proceeded to define a new dependent variable, F , in terms of the stream function, having the quality of depending solely on the transformation variable, η :

$$F(\eta) = \frac{\psi}{4 v_{\infty} x^{3/4} C}, \quad (25)$$

$$\eta = C x^{-1/4} \int_{\delta}^y \frac{dy}{\phi_{\mu}}, \quad (26)$$

where

$$C = \left(\frac{g}{4 v_{\infty}^2} \right)^{1/4} \quad (27)$$

and

$$\phi_{\mu} = \frac{\mu}{\mu_{\infty}} \quad (28)$$

In addition, one can express steam concentration, temperature, and aerosol population in terms of the normalized variables,

$$\xi = \frac{W - W_i}{W_{\infty} - W_i}, \quad (29)$$

$$\tau = \frac{T - T_i}{T_{\infty} - T_i}, \quad (30)$$

and

$$T = \frac{N - N_i}{N_{\infty} - N_i} \quad (31)$$

Making use of the following relations (cf. Minkowycz^[10]),

$$\left(\frac{\partial}{\partial x} \right)_y = \left(\frac{\partial}{\partial x} \right)_{\eta} - \left(\frac{\eta}{4x} + \frac{C}{x^{1/4} \phi_{\mu}} \frac{d\delta}{dx} \right) \left(\frac{\partial}{\partial \eta} \right)_x, \quad (32)$$

$$\left(\frac{\partial}{\partial y} \right)_x = \left(\frac{C}{x^{1/4} \phi_{\mu}} \frac{\partial}{\partial \eta} \right)_x, \quad (33)$$

$$u = \frac{4C^2 v_{\infty} x^{1/2} \pi}{\phi_{\mu}} F'(\eta), \quad (34)$$

$$v = \frac{C v_{\infty}}{x^{1/4}} \left(\eta \pi F'(\eta) - 3\pi F(\eta) + \frac{4C x^{3/4} \pi}{\phi_{\mu i}} \frac{d\delta}{dx} F'(\eta) \right), \quad (35)$$

Minkowycz and Sparrow transformed (4), (5), and (6) from the x, y domain into the η, x domain, resulting in an elimination of the x -variable:

$$\xi'' = -3 Sc \xi' F, \quad (36)$$

$$\left(\frac{\tau'}{\phi_{\mu}} \right)' = -3 Pr_{\infty} \left(\phi_c F + \frac{(\Delta W) \phi_{cvg}}{3Sc} \xi' \right) \tau', \quad (37)$$

$$\left(\frac{\pi F'}{\phi_{\mu}} \right)'' + 3F \left(\frac{\pi F'}{\phi_{\mu}} \right)' - \frac{2 \pi F'^2}{\phi_{\mu}} = \phi_{\mu} \left(1 - \frac{1}{\pi} \right). \quad (38)$$

Here the dependent variables are somewhat different from some of those chosen by Sparrow and Minkowycz. Also, the assumptions of constant k and Sc have entered the derivation.* A discussion of assumptions regarding the constancy of physical properties will appear in a later section.

Equation (12) also can be transformed to the η domain, the result being given by:

$$\beta \frac{Sc}{v_\infty} T'' = \Sigma_1 T' + \Sigma_2 \left(T + \frac{N_i}{N_\infty - N_i} \right), \quad (39)$$

where

$$\Sigma_1 = -\phi_\mu^2 \left[A_0 \pi + \frac{k\Delta T Sc}{5P v_\infty} \left(\frac{\tau'}{\phi_\mu} \right) \right] + \frac{2 \beta Sc \phi_\mu'}{v_\infty \phi_\mu}, \quad (40)$$

$$\Sigma_2 = -\phi_\mu^2 \left[A_0 (\pi' - \pi \Delta W q \xi') + \frac{k\Delta T Sc}{5P v_\infty} \left(\frac{\tau'}{\phi_\mu} \right)' \right], \quad (41)$$

$$A_0 = 3Sc F + (\Delta W) q \xi', \quad (42)$$

$$\beta = D \phi_\mu, \quad (43)$$

and

$$q = \frac{1}{W + \frac{1}{\sqrt{\frac{M_a}{M_w} - 1}}}. \quad (44)$$

Formulation of equation (39) incorporates the assumption of constant β , which, in view of Stokes-Einstein behavior, should not introduce appreciable error when temperature limits are small.

To complete a description of the system of transformed equations, an equation of state is required. Assuming ideal-gas behavior, one can satisfy this requirement by writing

$$\pi = \frac{(\Delta T) \tau + T_i}{T_\infty} \left[a + b (\Delta W) \xi + W_i \right], \quad (45)$$

where

*This contrasts with the work of Minkowycz and Sparrow, whose equations allowed for variable k and Sc .

$$a = \frac{M_W}{M_W - W_\infty (M_W - M_a)} \quad (46)$$

and

$$b = \frac{M_a - M_W}{M_W - W_\infty (M_W - M_a)}. \quad (47)$$

In equations (36) through (39) the primes denote differentiation with respect to the variable η ; hence the set of partial differential equations has been converted, through the similarity transformation, to an equivalent set of ordinary differential equations.

At this point the ultimate success of the similarity transformation depends on its ability to express the boundary conditions solely in terms of η . From equations (13), (14), (19), (20), (21), (22), and (23) it is obvious that

$$\tau = 0 \text{ at } \eta = 0, \quad (48)$$

$$\xi = 0 \text{ at } \eta = 0, \quad (49)$$

$$\Upsilon = 0 \text{ at } \eta = 0, \quad (50)$$

$$\tau = 1 \text{ at } \eta = \infty, \quad (51)$$

$$\xi = 1 \text{ at } \eta = \infty, \quad (52)$$

$$\Upsilon = 1 \text{ at } \eta = \infty, \text{ and} \quad (53)$$

$$F' = 0 \text{ at } \eta = \infty. \quad (54)$$

In addition, transformation of (17) provides the condition:

$$F = \frac{(\Delta W) \xi'}{3Sc (\Upsilon - W_i)} \text{ at } \eta = 0. \quad (55)$$

Finally, the no-slip condition (16) can be combined with (34) to give:

$$F' = \left(-\frac{q_t \delta \phi_\mu^2}{4 \lambda \mu_L \pi^2} \right)^{1/2} \text{ at } \eta = 0. \quad (56)$$

From Nusselt's derivation,

$$\delta = \left(-\frac{4 q_t v_L^2 x}{\lambda \mu_L g} \right)^{1/3}. \quad (57)$$

Hence,

$$F'' = \frac{\phi_{\mu}}{\pi} \left(-\frac{qt}{\lambda \mu_L} \right)^{2/3} \left(\frac{v_L}{4} \right)^{1/3} \left(\frac{x}{g} \right)^{1/6} \quad \text{at } \eta = 0. \quad (58)$$

Upon transforming (18) and substituting into (58), one obtains

$$F'' = r(s \tau'' + t \xi'')^{2/3} \quad \text{at } \eta = 0, \quad (59)$$

where

$$r = \frac{\phi_{\mu}}{2\pi} \left(\frac{v_L}{v_{\infty}} \right)^{1/3} (\lambda \mu_L)^{-2/3}, \quad (60)$$

$$s = k(\Delta T), \quad (61)$$

and

$$t = \frac{\mu \lambda (\Delta W)}{Sc (1 - W_i)}, \quad (62)$$

successfully transforming this final boundary condition into the η domain and completing the statement of the transformed problem.

WALL-FLUX EQUATIONS

Because of their usefulness for relating solutions of the boundary-layer problem to macroscopic system behavior, the wall-flux equations are of primary importance to this investigation. Formulated by performing material and energy balances at the gas-liquid interface, these equations may be written:

STEAM

$$\dot{m}_w = \left(w_{\rho v} - \rho D_{AB} \frac{\partial W}{\partial y} - w_{\rho u} \frac{d\delta}{dx} \right)_i \quad (63)$$

ENERGY

$$\dot{m}_h = \left(\rho u \frac{d\delta}{dx} (C_p T + \lambda W) - \left[\rho C_p T v - k \frac{\partial T}{\partial y} - \lambda \dot{m}_w \right] \right)_i \quad (64)$$

and AEROSOL

$$\dot{m}_p = \left(N \left(v - q D_{AB} \frac{\partial W}{\partial y} - \frac{k}{5P} \frac{\partial T}{\partial y} \right) - D \frac{\partial N}{\partial y} - Nu \frac{d\delta}{dx} \right)_i. \quad (65)$$

Transformed to the η domain, these become

STEAM

$$\dot{m}_w = -\frac{C}{x^{1/4}} \left[\frac{\mu_{\infty} \xi'' \Delta W}{Sc (1 - W)} \right]_i \quad (66)$$

ENERGY

$$\dot{m}_h = - \frac{C}{x^{1/4}} \left[\frac{\lambda \mu_\infty (\Delta W)}{Sc (1 - W)} \xi' + \frac{C_p \mu_\infty (\Delta T) \tau'}{Pr} \right]_i \quad (67)$$

and AEROSOL

$$\dot{m}_p = - \frac{C}{x^{1/4}} \left[\left(3\pi v_\infty F + \frac{\pi q v_\infty \Delta W}{Sc} \xi' + \frac{C_p \mu_\infty \Delta T}{5P Pr} \tau' \right) N + \frac{\beta N'}{\phi_\mu^2} \right]_i \quad (68)$$

ESTIMATION OF PHYSICAL PROPERTIES

Physical properties of air and steam were obtained from the literature and combined to estimate mixture properties, using recommended methods.^[14] A listing of the estimated values is given in Appendix 3, along with a tabulation of the sources.

Variation of specific heat and viscosity across the boundary layer was approximated by assuming these properties to be proportional to the mass fraction of steam. These approximations resulted in insignificant error, owing the small differences in temperature and to the similar shapes of the temperature- and steam-concentration profiles.

Variation of density, as discussed previously, was assumed to follow ideal-gas behavior. Thermal conductivity and Schmidt number did not vary significantly across the boundary layers, and were taken to be constant during each solution of the boundary-layer problem.

SOLUTION OF BOUNDARY-LAYER EQUATIONS

The boundary-layer equations (36), (37), (38) and (39), subject to the boundary conditions (48) - (55) and (59), constitute a boundary-value problem composed of coupled, nonlinear equations. Solution of such problems by present-day computational methods demands that some type of iterative technique be employed. Such techniques can be categorized roughly into two classes. The first of these involves linearization using approximating functions which are re-estimated after each iteration. The second class of methods entails estimation of the missing initial conditions (boundary conditions at $\eta = 0$), and solving the

resulting initial-value problem, with subsequent re-estimation of the initial conditions after each iteration.

For complex systems of coupled nonlinear equations, convergence schemes are normally quite complicated, and numerical algorithms designed to lead such systems toward convergence are likely to be inefficient and time-consuming. For this reason, a hybrid-computer technique was chosen for solution of the present problem. This technique combined the capability of rapid iterative solution with the advantage of manual adjustment of the initial conditions, thereby enabling an adequate degree of convergence to be attained in a comparatively short time.

The rather complicated algebra of equations (40) and (41) made it expedient to solve them digitally. The remaining segments of the boundary-value problem were processed on the analog portion of the hybrid computer. Figure 3 gives a schematic of the hybrid system. This system was composed of a Beckman 2133 analog computer interfaced with a Digital Equipment Corporation PDP-7 digital computer operated by the Simulation Section of Battelle-Northwest Laboratory. A chart showing the analog network is given in Appendix 1.

Inspection of equation (39) shows that it may be solved independently of the remaining equations provided Σ_1 and Σ_2 are known. Moreover, knowledge of these variables renders equation (39) linear in form, allowing its solution to be accomplished rapidly using conventional numerical techniques. Solution of equation (39) in this manner has the additional advantage of not occupying the hybrid computer for long periods of time while iterations on equation (39) are performed; for these reasons hybrid solutions of equation (39) were restricted to preliminary determinations. All subsequent computations of particle profiles were performed digitally using Σ_1 and Σ_2 furnished by the hybrid computer. Tabulations of Σ_1 and Σ_2 are given in Appendix 2. The finite-difference equations used for solution of equation (39) are listed in Appendix 1.

The majority of time expended in solving the total boundary-value problem was spent on scaling the analog to achieve optimal results. Once set up, the system permitted convergence to be approached adequately within a five minute period.

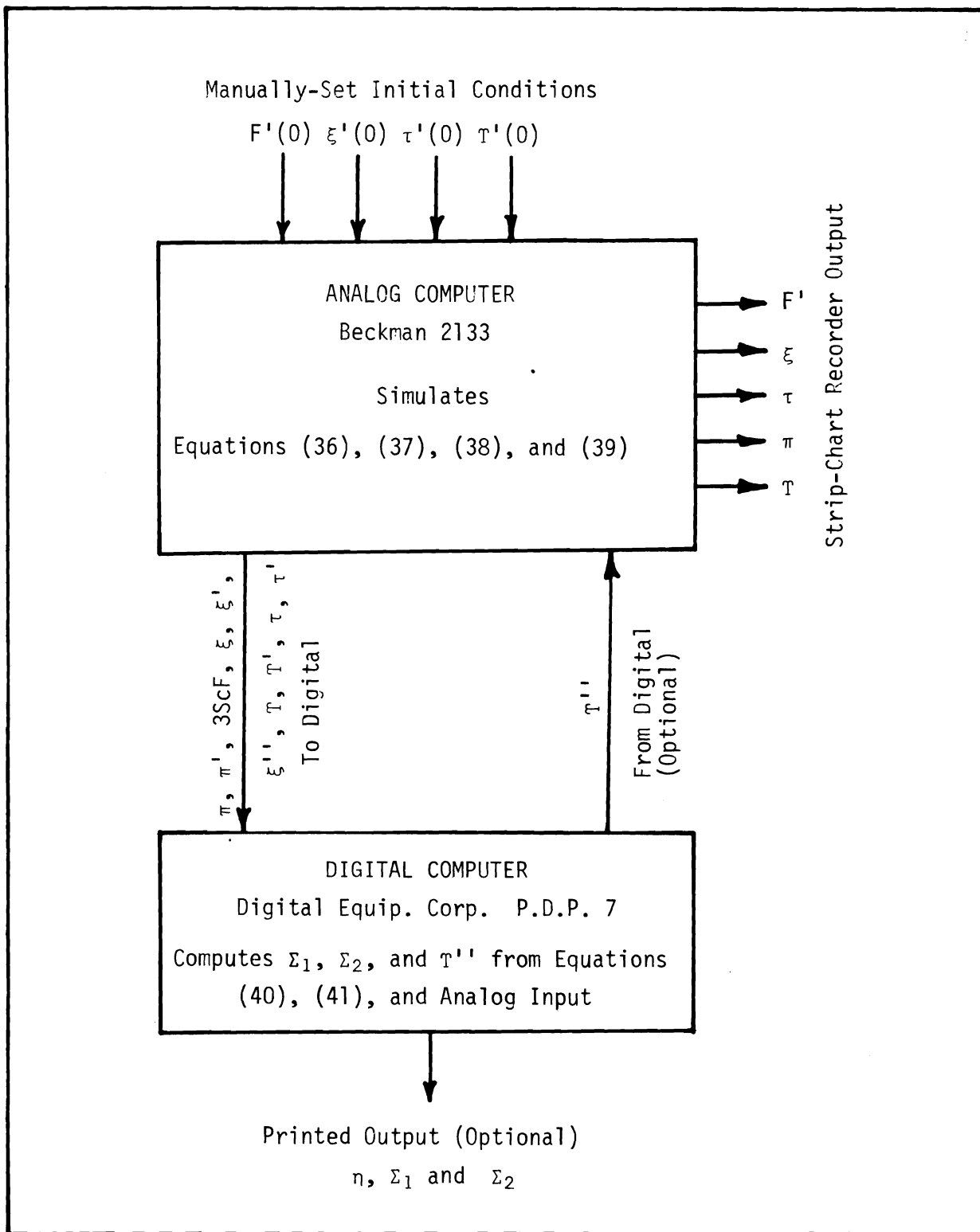


FIGURE 3

SCHEMATIC OF COMPUTATIONAL LAYOUT

RESULTS

Solutions of Steam, Energy, and Momentum Transport Equations

As discussed previously, the equations for steam, energy, and momentum transport could be solved independently of the particle-transport equations. Such solutions were obtained for each of the conditions shown in Table I. The range of variables listed in Table I was chosen because it was believed to be representative of conditions expected in post-accident containment systems. Bulk and interfacial mixtures were maintained at saturation for all conditions studied. The results of these computations are shown in Figures 4 through 12. The points on the curves were generated by a digital computer solution which was performed to check the analog results. A discussion of this check will be presented in the following section.

The variables Σ_1 and Σ_2 were computed for the conditions listed in Table I as well. These were obtained as digital print-out from the hybrid computer, and are given in Appendix 2.

Solutions of Particle-Transport Equation

Solutions of the particle-transport equation, as discussed previously, were obtained through the finite-difference approximations given in Appendix 1. These equations were solved using a Univac 1108 digital computer operated by the Computer Sciences Corporation. Various solutions to equation (39), corresponding to hybrid runs 1-1, 1-4, and 1-16 appear in Figures 13, 14, and 15. Steep slopes of the particle profiles in the vicinity of the interface necessitated use of a rather fine grid spacing in this area; wider grid spacings could be employed for other regions, with negligible loss of accuracy. Grid spacings for the present numerical evaluation were chosen to approximate the solutions so that truncation error was less than 0.2 percent. Grid spacings for each of the solutions are given in Table II.

TABLE I

PHYSICAL CONDITIONS FOR COMPUTED RESULTS

<u>Run*</u>	<u>$T_{\infty} - T_i$ (°R)</u>	<u>P_{steam} (ATM)</u>	<u>T_{∞} (°R)</u>
0.5-1	1	.5	638.7
0.5-2	2	.5	638.7
0.5-4	4	.5	638.7
0.5-8	8	.5	638.7
0.5-16	16	.5	638.7
1-1	1	1	671.7
1-2	2	1	671.7
1-4	4	1	671.7
1-8	8	1	671.7
1-16	16	1	671.7
2-1	1	2	708.7
2-2	2	2	708.7
2-4	4	2	708.7
2-8	8	2	708.7
2-16	16	2	708.7

Air pressure in atmospheres is equal to $(T_{\infty}, \text{°R})/539.7$ for all cases, corresponding to base conditions of one atmosphere air at 80°F.

* First term in run number designates bulk steam pressure in atmospheres. Second term denotes $T_{\infty}-T_i$, °F.

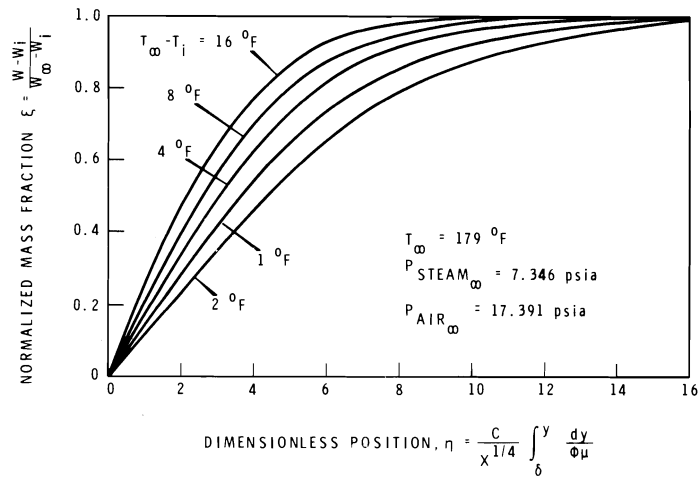
TABLE II

GRID SPACINGS USED FOR FINITE-DIFFERENCE APPROXIMATION OF PARTICLE-TRANSPORT EQUATION

<u>Run*</u>	<u>$\Delta\eta$ Initial</u>	<u>Position Of Grid Enlargement $\eta=$</u>	<u>$\Delta\eta$ Final</u>
1-1-.01	0.05	4.0	0.5
1-4-.01	0.01	1.0	0.5
1-16-.01	0.002	0.4	0.1
1-1-.05	0.01	1.0	0.5
1-4-.05	0.001	0.2	0.5
1-16-.05	0.0002	0.04	0.1
1-1-.1	0.001	0.4	0.5
1-4-.1	0.0005	0.1	0.5
1-16-.1	0.00005	0.015	0.1

* Last term refers to aerosol particle diameter in microns. Other terms are as indicated in Table I.

FIGURE 4



COMPUTED STEAM CONCENTRATION PROFILES ADJACENT TO A FLAT, VERTICAL PLATE

FIGURE 5

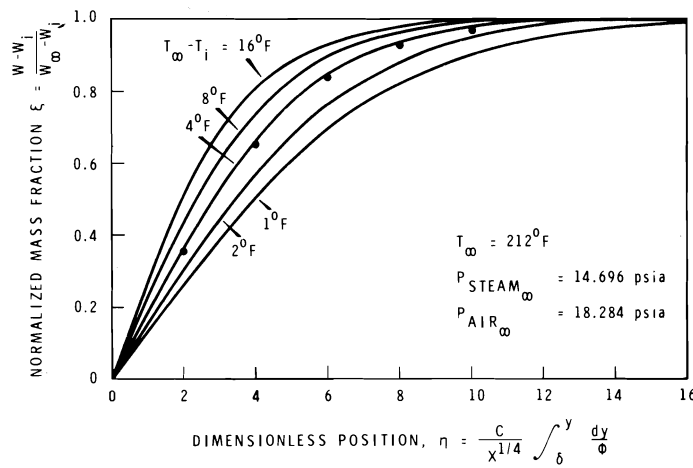
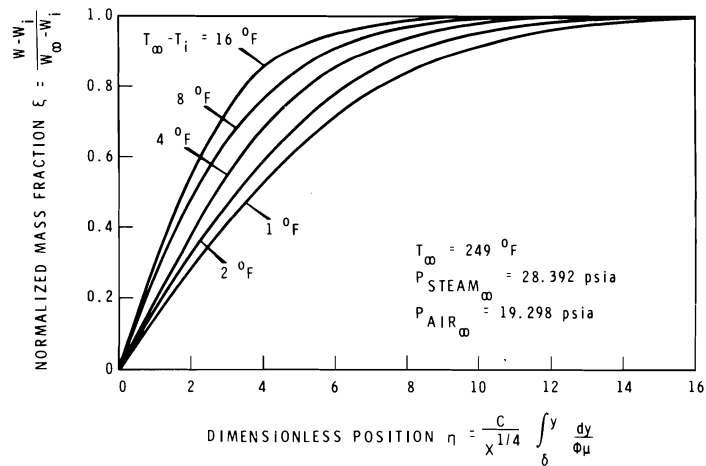
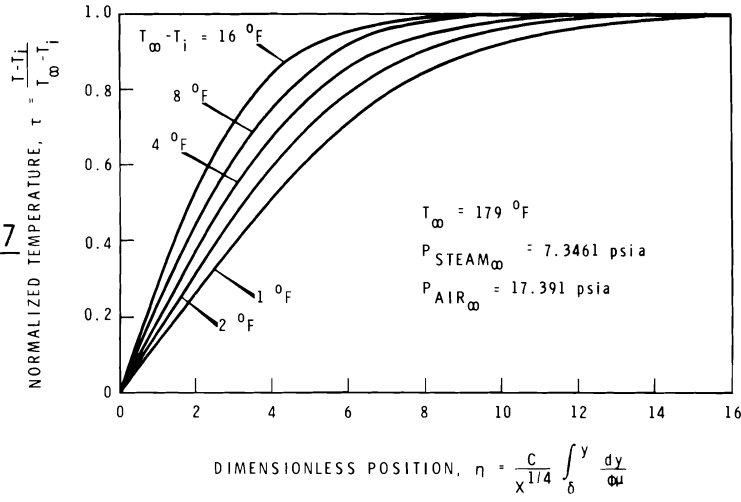


FIGURE 6



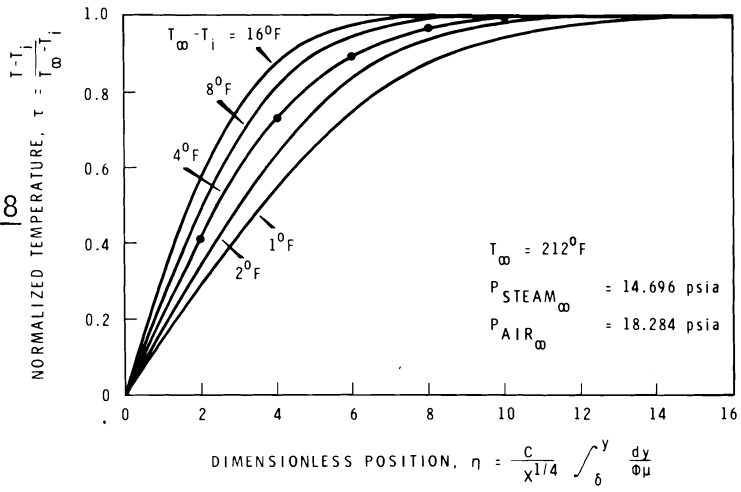
COMPUTED STEAM CONCENTRATION PROFILES IN GASEOUS BOUNDARY LAYER

FIGURE 7



COMPUTED TEMPERATURE PROFILES ADJACENT TO A FLAT, VERTICAL PLATE

FIGURE 8



COMPUTED TEMPERATURE PROFILES IN GASEOUS BOUNDARY LAYER

FIGURE 9

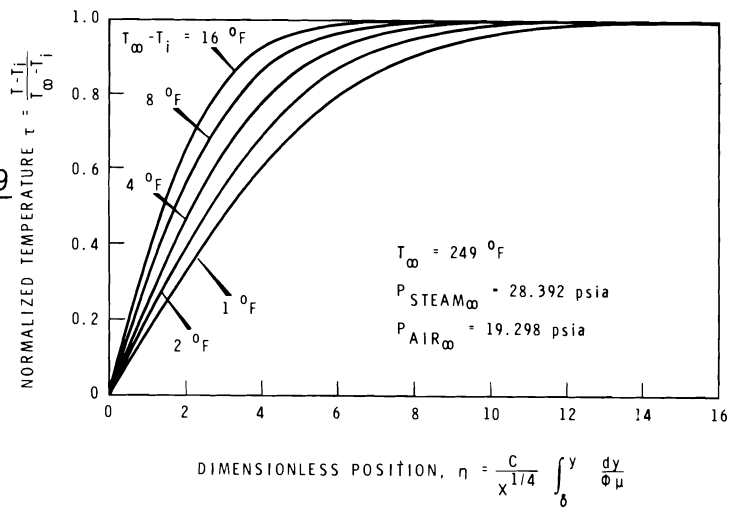


FIGURE 10

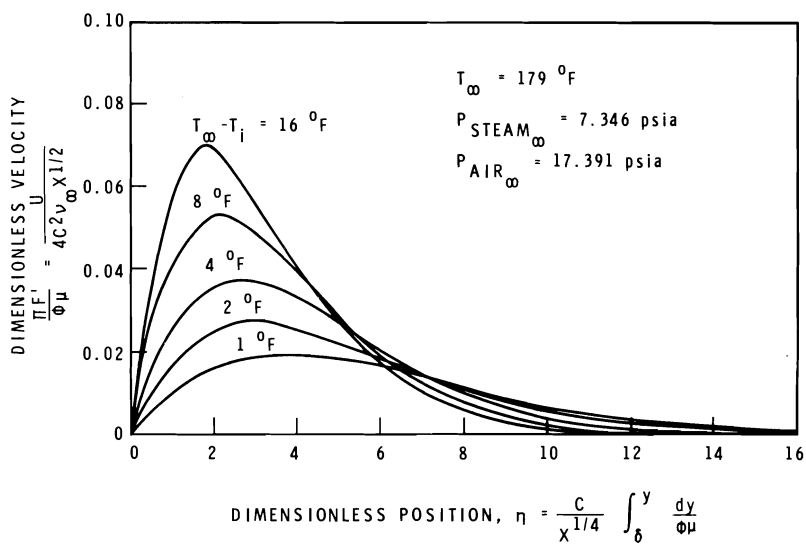


FIGURE 11

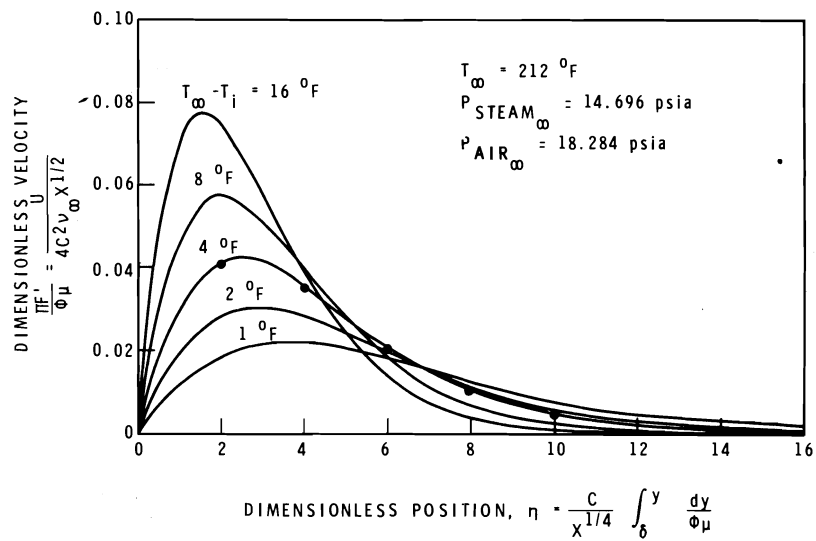
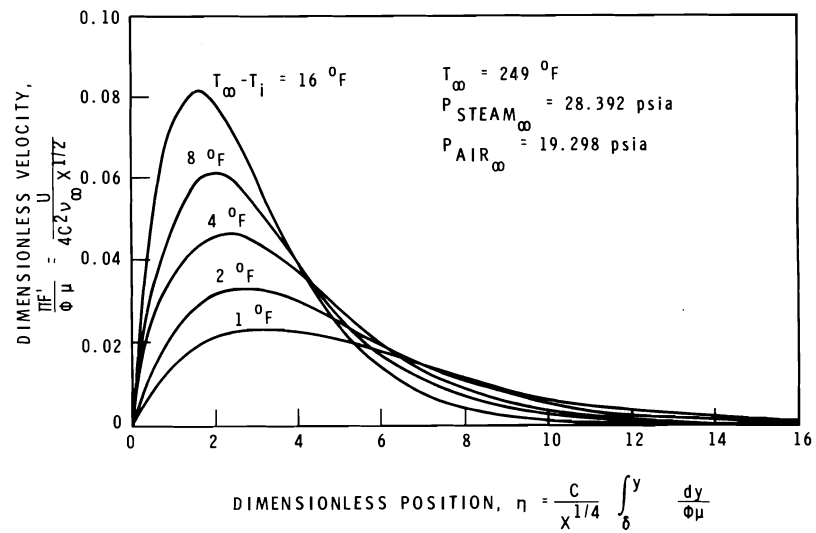


FIGURE 12



COMPUTED VELOCITY PROFILES IN
GASEOUS BOUNDARY LAYER

FIGURE 13

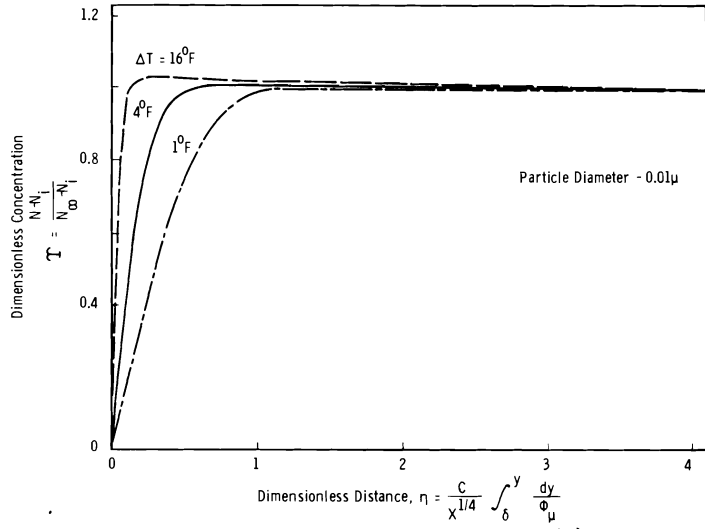


FIGURE 14

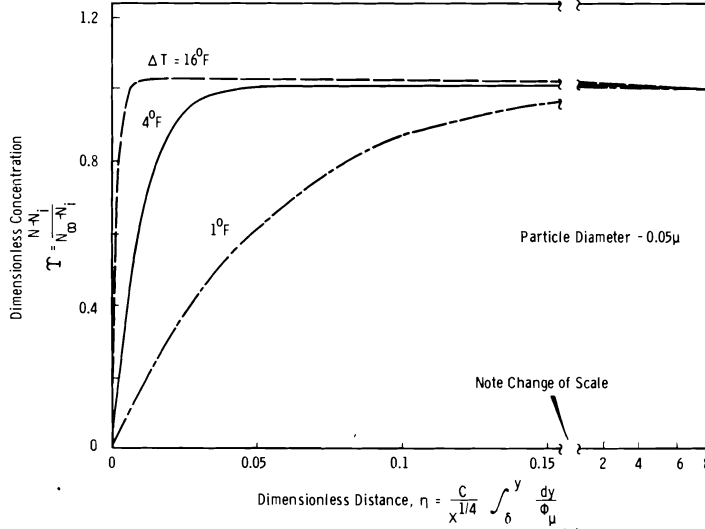
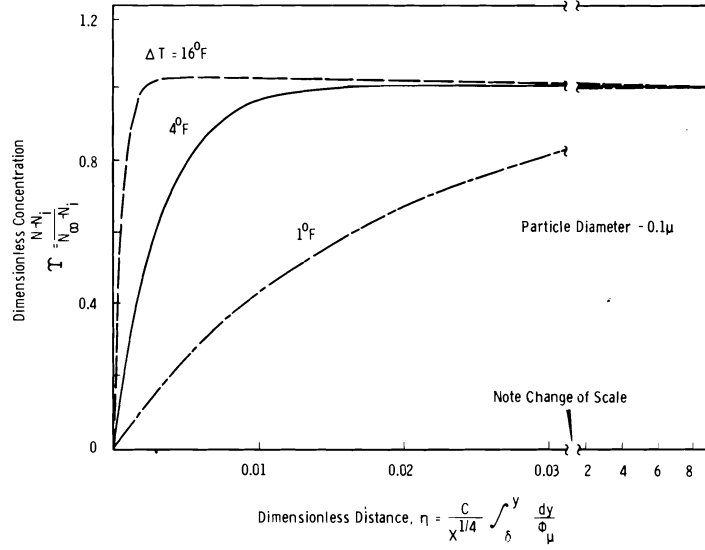


FIGURE 15



COMPUTED PARTICLE CONCENTRATION PROFILES IN GASEOUS BOUNDARY LAYER

Wall Transport Calculations

Transport rates of energy, steam, and aerosol to the liquid-vapor interface can be calculated directly from the computed results using relations (66) through (68). Interfacial fluxes determined in this manner are shown in Tables III and IV. Here the fluxes are multiplied by the factor $x^{1/4}$ to eliminate x -dependence, in conformity with the similarity transformation. Aerosol-deposition fluxes have been calculated assuming a perfect sink at the interface, i.e., $N = 0$ at $\eta = 0$.

Humidity in the Boundary-Layer Region

The question of whether or not saturation exists in the boundary-layer region is of primary importance to this investigation. If supersaturation exists, the basic governing equations will not apply, since they do not allow for condensation in regions other than at the liquid-vapor interface. Furthermore, supersaturation in the boundary-layer region would almost certainly cause particle growth by condensation, invalidating many of the assumptions made in formulating the particle-transport equation.

For given conditions of temperature and pressure, the saturation curve can be represented as a plot of τ versus ξ , as shown by the dashed line in Figure 16. Area above the dashed line corresponds to subsaturated conditions, while that below the line indicates conditions wherein supersaturation exists. Plotting τ versus ξ from the computed results produces lines that fall above the saturation curve, indicating a distinct tendency toward subsaturation in the boundary layer. Figure 16 shows a curve corresponding to a single set of bulk and interface conditions; however, the indicated tendency toward subsaturation was observed in each of the cases studied.

Owing to the relative magnitudes of the Schmidt and Prandtl numbers, one might intuitively expect the noted trend toward subsaturation. However, the rather complex interactions between the various transport mechanisms render such an intuitive prediction of doubtful validity, necessitating this more exact type of analysis to determine true physical behavior.

Particle Trajectories

For visualization purposes, it is interesting to observe the path of an aerosol particle from the point it enters the boundary layer to the point it impinges on the liquid interface. The equation describing the path is given by:

TABLE III

COMPUTED FLUXES OF ENERGY AND STEAM AT LIQUID-VAPOR INTERFACE

<u>Run</u>	ξ_i'	τ_i'	$-\dot{m} \times 1/4$ <u>lbm/ft^{7/4} hr</u>	$-\dot{m} \times 1/4$ <u>BTU/ft^{7/4} hr</u>
0.5-1	0.119	0.135	0.00858	8.84
0.5-2	0.143	0.161	0.0202	20.9
0.5-4	0.170	0.195	0.0463	47.9
0.5-8	0.205	0.235	0.104	108.
0.5-16	0.245	0.287	0.219	230.
1-1	0.127	0.149	0.0177	17.6
1-2	0.152	0.179	0.0414	41.3
1-4	0.182	0.218	0.0946	94.5
1-8	0.223	0.268	0.213	214.
1-16	0.267	0.338	0.436	442.
2-1	0.134	0.163	0.0371	35.7
2-2	0.160	0.198	0.0859	82.7
2-4	0.197	0.244	0.198	191.
2-8	0.243	0.312	0.436	423.
2-16	0.299	0.406	0.872	856.

TABLE IV

COMPUTED AEROSOL DEPOSITION FLUXES*

<u>Run</u>	τ_i'	$\frac{-\dot{m}_a \times 1/4}{N_\infty}$ <u>ft^{5/4} hr</u>
1-1-.01	2.00	.412
1-1-.05	18.9	.201
1-1-.1	55.7	.197
1-4-.01	6.01	1.21
1-4-.05	103.8	1.08
1-4-.1	311.	1.08
1-16-.01	29.2	5.45
1-16-.05	560.	5.38
1-16-.1	1681.	5.37

* Per unit bulk concentration.

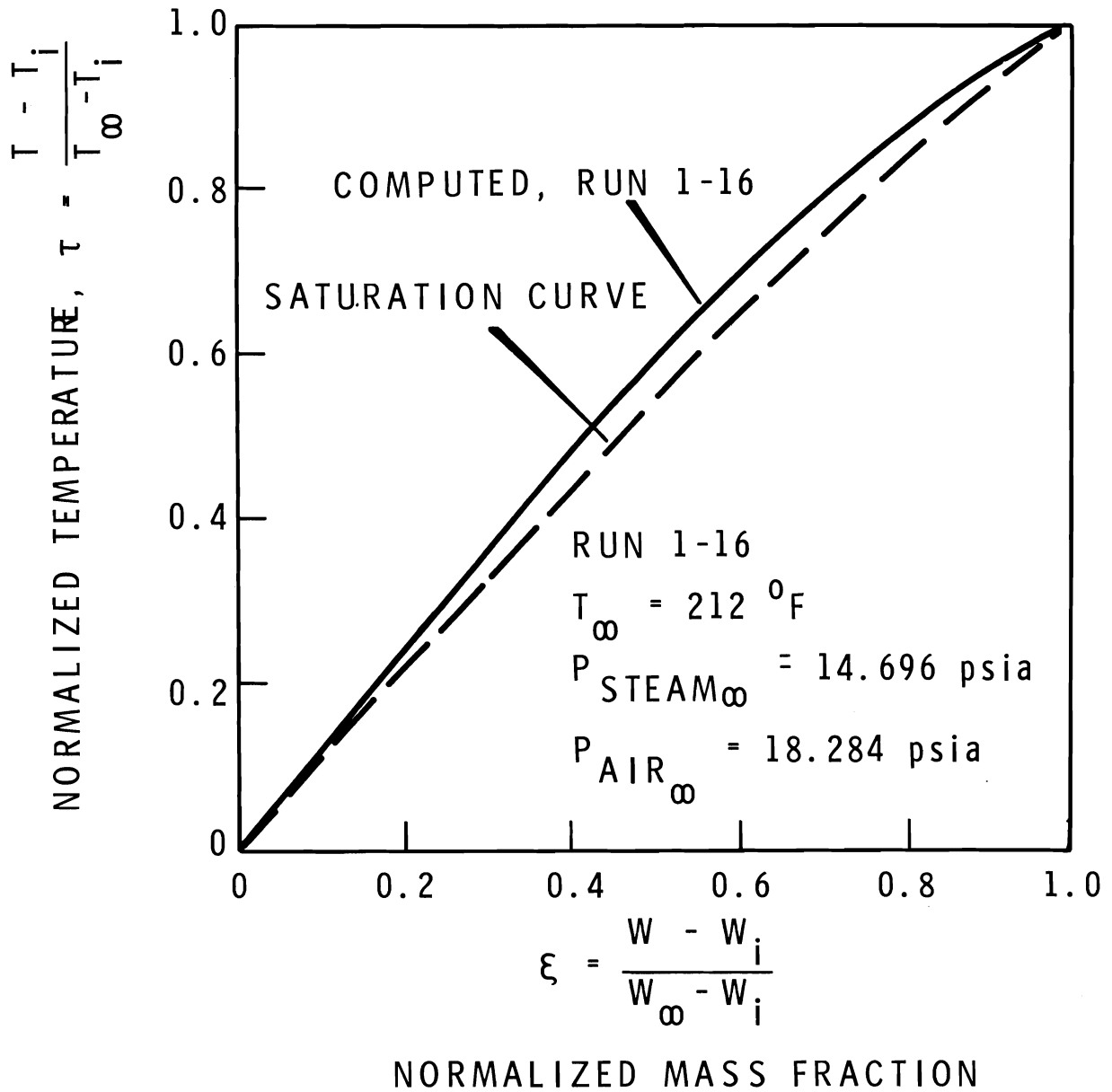


FIGURE 16

HUMIDITY RELATIONSHIPS IN GASEOUS BOUNDARY LAYER

$$x = \int_{\delta}^y \frac{dx}{dy} dy = \int_{\delta}^y \frac{u(x,y)}{v_p(x,y)} dy, \quad (69)$$

where u and v_p are the velocities of the particle in the x and y directions as described previously.

Except for regions very close to the interface, particle diffusion and growth of the liquid film have little effect on v_p . Assuming these entities to be negligible, the relation

$$v_p = \frac{C v_{\infty} \pi}{x^{1/4}} \left(\eta F' - 3F - \frac{\Delta W \xi'}{Sc f(\xi)} - \frac{\Delta T k \tau'}{5v_{\infty} P \phi_{\mu} \pi} \right). \quad (70)$$

may be written, where

$$f(\xi) = \Delta W \xi + W_i + \frac{1}{\sqrt{\frac{M_a}{M_w} - 1}}. \quad (71)$$

Combining with equations (34) and (69), and neglecting the effects of varying viscosity and density, one may write the following approximate differential equation describing the particle trajectory:

$$\frac{dx}{dy} = \frac{4C x^{3/4} F'}{\eta F' - 3F - \frac{\Delta W \xi'}{Sc f(\xi)} - \frac{\Delta T k \tau'}{5v_{\infty} P}}. \quad (72)$$

Equation (72) was solved numerically using interpolated values from the hybrid-computer output. A fourth-order Runge-Kutta technique was employed^[2], which started at some point on the interface and computed the trajectory backwards to the edge of the boundary layer.

Curves for several of these computations are shown in Figure 17. These are expected to be quite accurate for particles larger than about .02 microns in diameter, where the neglect of Brownian diffusion is justified. Some of these curves undoubtedly protrude into turbulent boundary-layer conditions, and must be considered invalid at points where nonlaminar situations exist. In this context, it is interesting to note that many of the particles entering the laminar boundary layer will deposit under turbulent conditions, passing into the turbulent regime somewhere along their traverse to the wall.

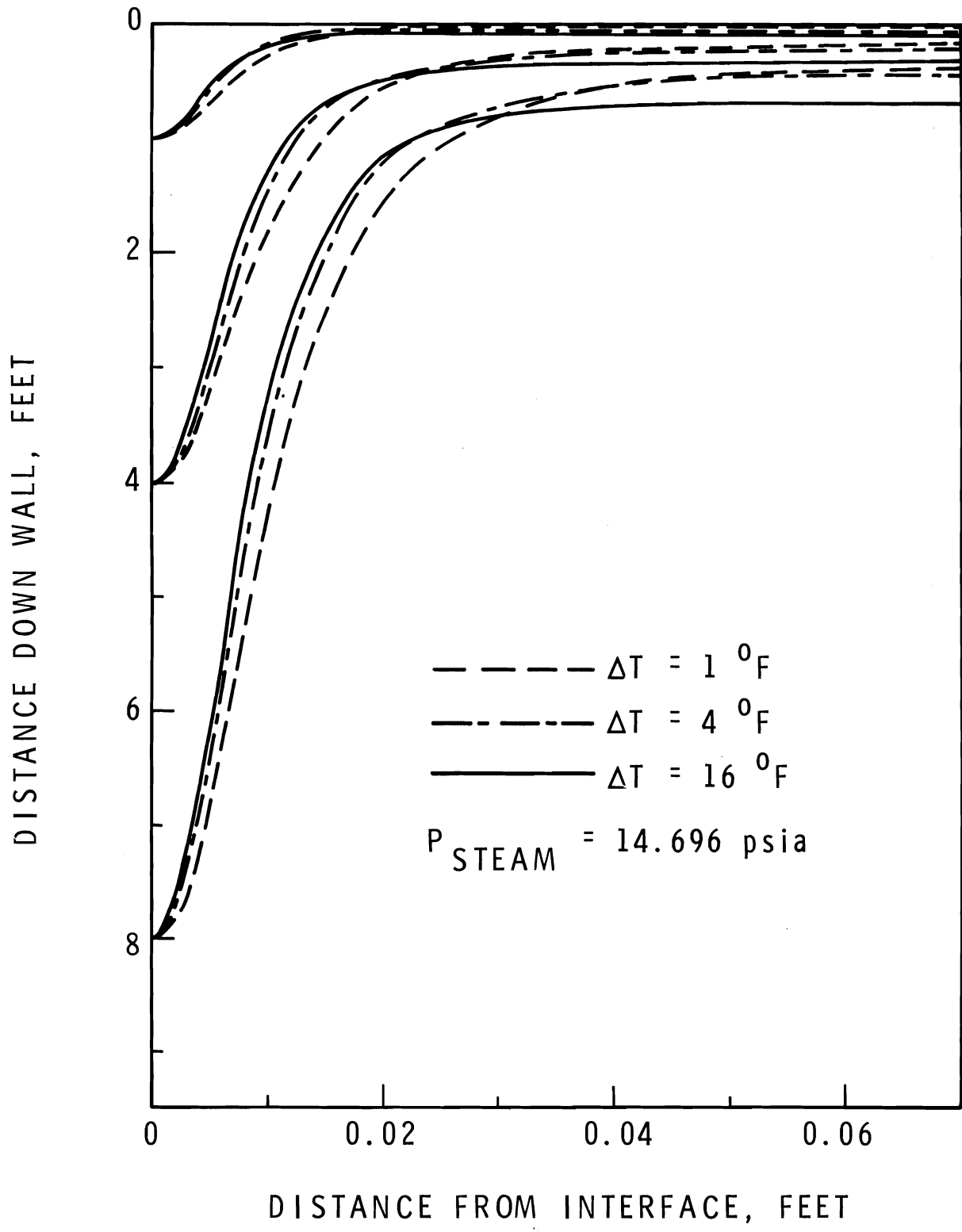


FIGURE 17

ESTIMATED PARTICLE TRAJECTORIES

DISCUSSION OF RESULTS

Validity of Equations

Equations (36), (37) and (38), describing steam, energy, and momentum transport in a laminar boundary layer, are believed to be based upon a highly realistic model of physical behavior. Although no experimental profile-data have been published to test these equations directly, one can refer to previous comparisons of theory with experimental results for non-condensing systems. Such comparisons^[15] show agreement between experiment and theory to be quite good -- certainly within the errors of experimental measurement.

The assumptions that Nusselt's equation is a valid description of liquid-film behavior, and that interfacial temperature is constant might be somewhat in question; however, these assumptions may be expected to be reasonably valid whenever the rate-influencing significance of the liquid film is small compared to that of the gaseous boundary layer.^[6] Temperature drop across the liquid film may be computed on the basis of Nusselt's theory using the following expression:

$$T_w - T_i = \frac{(\dot{m}_h x^{1/4})^{4/3}}{k_L} \left(\frac{4v_L}{\lambda g \rho_L} \right)^{1/3} \quad (73)$$

Values of liquid-film temperature-drop for each of the conditions studied were calculated from equation (73), and are presented in Table V. From the low magnitudes of these values it is apparent that the assumptions of Nusselt-type behavior and constant interfacial temperature are totally credible for all practical applications of the present study.

TABLE V

LIQUID-FILM TEMPERATURE-DROPS CALCULATED FROM NUSSELT THEORY

$T_\infty - T_i^*$ °F	$T_i - T_w^{**}$, °F		
	Run Series 0.5-	Run Series 1-	Run Series 2-
1	.00244	.00571	.0142
2	.00767	.0176	.0418
4	.0240	.0535	.130
8	.0690	.160	.375
16	.192	.423	.968

* Across gaseous boundary layer.

** Across liquid film.

Boundary conditions (48) and (49) state that the interfacial temperature and composition are in equilibrium in the liquid and gaseous phases. This is not quite true, since continuum mechanics break down in the range of a mean-free-path from the interface, giving rise to an apparent discontinuity, or "jump" in temperature. For the conditions imposed in the present study, however, the significance of interfacial resistance has been shown to be negligibly small.^[10]

An additional point of interest is the stipulation that the bulk be maintained at saturation. This seems a reasonable assumption with respect to containment vessel analysis, since the supply of steam should tend to keep the interior of the vessel close to one hundred percent relative humidity. Nevertheless, the behavior exemplified in Figure 16 indicates a distinct tendency of the condensation process to lead the bulk toward subsaturation. Limited subsaturation should not affect heat and mass transfer rates appreciably; hence, the saturated-bulk assumption is not considered to be a serious one so far as the present investigation is concerned.

Equation (39), describing aerosol transport through the condensing-steam boundary-layer, is thought to be somewhat less accurate than its counterparts in describing physical behavior. The comparatively high diffusivities of steam and thermal energy render equations (36) and (37) rather insensitive to minor perturbations in flow patterns; however, such perturbations would not have to be large to create effective particle diffusion-coefficients in excess of those resulting from Brownian motion. A corollary of this is that the validity of equation (39) should tend to increase as the particle size decreases (as Brownian diffusivity increases).

It should be pointed out that while the above-mentioned difficulties possibly could cause significant deviations between actual and computed aerosol concentration profiles, the resulting deposition rates would not be altered appreciably. This arises from the fact that while particle diffusion is important in establishing the concentration profiles, diffusiophoresis is still the most prominent mechanism of mass transfer. A discussion of the relative importance of the various particle-transport mechanisms will be given in a following section.

In discussing the validity of equation (39) it is interesting to note the predicted aerosol-concentration buildup in the boundary-layer region, as shown in Figures 13, 14, and 15. Analysis of the equation shows that such a

buildup can occur only if Σ_2 is non-zero. Non-zero Σ_2 occurs for several reasons. First, the terms involving $(\Delta W) q \xi'$ occur because of differentiation of the aerosol flux arising from the diffusiphoretic correction factor. The additional term containing τ' arises from a similar differentiation of the thermophoretic contribution. If these terms were neglected, (41) would take the form,

$$\Sigma_2 = - \phi_{\mu}^2 \pi' (3ScF). \quad (74)$$

This remaining term arises because the expression for particle diffusion was written in terms of a concentration gradient rather than a mass-fraction gradient, as was the case for diffusion of steam. Expressed as the flux of particles passing a reference frame moving with the mass-average velocity, this expression is

$$J_p = - D \frac{dN}{dy}. \quad (75)$$

Equation (75) was chosen rather arbitrarily by Einstein^[5] for use in his formulation of the Stokes-Einstein equation. For systems wherein density is constant this expression is equivalent to the form

$$J_p = - \frac{D_p}{m_p} \frac{dW_p}{dy}, \quad (76)$$

where W_p is the particle mass-fraction and m_p is the mass of a single particle. This is not the case, however, for the present situation, wherein variations in density are significant.*

Although equation (76) has a certain amount of intuitive appeal, both expressions must be regarded as somewhat phenomenological in nature, and the true significance of the term $\pi' (3ScF)$ in equation (41) is doubtful.

Significance of the contributions by thermophoresis and the diffusiphoretic correction factor is also subject to some conjecture. During the derivation of equation (39), the y-component of particle velocity was taken as equal to the following sum:

$v_p =$ mass-average velocity + particle diffusion velocity,
relative to mass-average velocity + velocity corresponding
to diffusiphoretic correction term + thermophoretic velocity.

* It should be noted here that if Einstein had chosen a phenomenological form of Fick's law based on a mass-fraction driving force, his expression for the diffusion coefficient would not have taken the form $D = 1/6\pi\mu r$. This has not been recognized explicitly in a majority of the published literature (cf [1]).

This implies an additive relationship between each of the mechanisms. It also depends on the assumption of pseudo-binary diffusion. In view of the obvious interactions of the mechanisms, these assumptions are not strictly valid; however, there is little reason to expect that they should not apply with reasonable accuracy under the present circumstances.

There are several other possible criticisms of equation (39). The assumption of constant particle size precludes the assessment of particle-growth effects arising from nucleation and coagulation. Nucleation effects are expected to be insignificant because of the saturation relationships in the boundary layer exemplified by Figure 16. Coagulation, which depends on particle population density, should be negligible during most of the post-accident period when equation (39) is otherwise applicable.

The boundary condition (19), giving aerosol concentration at the liquid-vapor interface, also is subject to some conjecture. In the present study the interfacial aerosol concentration was taken to be zero, implying a perfect sink for particles at $\eta = 0$. Because of the nature of the wet surface, such an assumption should be reasonably valid, especially for water-soluble aerosols.

From the above discussion it is concluded that equation (39) and its boundary conditions present a reasonably valid model of aerosol transport, provided the boundary layer is truly laminar. Shapes of the predicted concentration profiles may not be as accurate as the predicted deposition rates, owing to the overwhelming importance of diffusiophoresis as a particle-transport mechanism. The concentration build-up predicted by equation (39) is probably a real phenomenon, although there are several uncertainties pertaining to its physical origin.

Accuracy of Computations

Accuracy of solutions to the boundary-layer equations was limited primarily by performance of the analog-computer components. Normally taken to be within one percent, machine error can accumulate seriously if large numbers of nonlinear components are involved, or if a poor choice of scaling parameters is employed. Scale factors used in the present computations are given in Appendix 1. These were chosen carefully so as to maximize accuracy of the computations.

A digital-computer program was written to estimate magnitudes of the analog-computer errors. This program employed the initial conditions deter-

mined by the analog computer to solve equations (36) through (41), using a fourth-order Runge-Kutta technique.^[2] A step size $\Delta\eta = 0.1$ was found to be sufficient for adequate convergence of the Runge-Kutta analysis.

Comparison of the results obtained from both types of computers (run 1-4) showed analog-computer errors to be generally less than one percent. Comparison of the results is presented graphically in Figures 5, 8, and 11.

Values of Σ_1 and Σ_2 , computed digitally from the analog results, were subject to all of the associated sources of error. Σ_2 resulted from a subtraction of variables, and this often served to amplify deviations between its real and computed values. Errors in Σ_1 are expected to be on the order of two percent, while corresponding errors in Σ_2 may be as high as five percent.

Finite-difference approximations of the particle-concentration profiles were performed so as to converge to within 0.2 percent. Therefore, the major source of error in these computations arose from uncertainties in Σ_1 and Σ_2 . Owing to the small relative magnitude of Σ_2 , its errors did not affect the concentration-profile values to an appreciable extent. Therefore, the expected errors in the computed concentration values should be on the order of one or two percent of the corresponding maximum values.

Simplified Analysis of Heat and Vapor Transport -- Test of Heat Transfer-Mass Transfer Analogy

Transport of vapor and energy in a condensing-steam boundary layer occurs by processes that are roughly analogous. Because of this, it is possible to perform a simplified analysis of heat and vapor transport in condensing systems, based on known behavior of heat transfer in noncondensing boundary layers. Such an analysis is possible for both laminar and turbulent regimes.^[9]

For laminar, noncondensing boundary layers formed adjacent to flat, vertical plates, theory has indicated^[15] that the Nusselt number, Nu, should possess the following functional dependence on the Grashoff and Prandtl numbers:

$$\text{Nu} = .388 [\text{Gr} \cdot \text{Pr}]^{1/4}. \quad (77)$$

This compares well with the expression

$$\text{Nu} = .416 [\text{Gr} \cdot \text{Pr}]^{1/4}, \quad (78)$$

which was obtained on the basis of experimental heat-transfer data.

The Sherwood (Sh) and Schmidt numbers are the mass-transfer analogs of

the Nusselt and Prandtl numbers; hence the mass-transfer analog of equation (77) is:

$$Sh = .388 [Gr \cdot Sc]^{1/4}. \quad (79)$$

The corresponding interfacial steam flux can be calculated using the definition of the mass-transfer coefficient, combined with the film-theory correction factor of Stewart.^[1] Given here without derivation, this is

$$\dot{m}_w = - \frac{\rho D_{AB}}{x} Sh \frac{\Delta W}{(1 - W_i)} \frac{\theta_w}{e^{\theta_w} - 1}, \quad (80)$$

where

$$\theta_w = \ln \frac{1 - W_\infty}{1 - W_i}. \quad (81)$$

A similar equation can be written for the conduction heat-flux at the interface. This is:

$$\dot{m}_h^0 = - \frac{k}{x} Nu (T_\infty - T_i) \frac{\theta_h}{e^{\theta_h} - 1}, \quad (82)$$

where

$$\theta_h = \frac{\dot{m}_w C_{pw} x}{k Nu}. \quad (83)$$

One should note that \dot{m}_h^0 is the heat flux arising from conduction alone, and that the total interfacial flux of thermal energy is given by:

$$\dot{m}_h = \dot{m}_h^0 + \lambda \dot{m}_w. \quad (84)$$

Validity of the analogy was tested by comparing mass and energy fluxes calculated through equations (80) and (81), with those obtained from the computer solutions of the boundary-layer equations on the basis of equations (66) and (67). This comparison is shown in Table VI, which gives ratios of interfacial fluxes predicted by the two methods of analysis. Table VI indicates that the heat transfer-mass transfer analogy is valid with a surprisingly high degree of accuracy for laminar-flow conditions. It also implies strongly that such an analogy should apply accurately under turbulent conditions as well.

Finally, it should be noted that the theoretical equation (77) was used as a basis for comparison, rather than equation (78), which was obtained from experimental data. Since these equations agree to within about ten percent,

the analogy is regarded as highly satisfactory no matter which is employed for comparison. Edge effects in experimental heat-transfer measurements would tend to make the resulting data somewhat high; hence equation (77) was thought to be a somewhat more logical basis for testing the analogy.

TABLE VI

RATIO OF TRANSFER RATES CALCULATED BY ANALOGY WITH PURE HEAT
TRANSFER TO RATES CALCULATED FROM COMPUTER SOLUTION

Run	$\frac{\dot{m}_w \text{ analogy}}{\dot{m}_w \text{ computer}}$	$\frac{\dot{m}_h \text{ analogy}}{\dot{m}_h \text{ computer}}$
2-1	0.99	0.94
2-2	1.00	0.94
2-4	0.99	0.94
2-8	0.99	0.94
2-16	1.00	0.93
1-1	1.00	0.97
1-2	1.00	0.96
1-4	1.00	0.96
1-8	0.99	0.96
1-16	1.01	0.96
0.5-1	0.99	0.98
0.5-2	0.99	0.98
0.5-4	0.99	0.98
0.5-8	0.99	0.99
0.5-16	1.00	1.00

Simplified Analysis of Aerosol Transport

In the absence of solutions to the boundary-layer equations, one might conceivably attempt to estimate particle deposition rates on the basis of steam condensation, assuming the aerosol to be swept to the wall with the mass-average velocity of the fluid. Such an approach is particularly appealing, since mass-average velocity can be estimated simply by measuring condensation rates, or by applying the analogy discussed in the preceding section. In accordance with the boundary-layer analysis, mass-average velocity at the liquid-vapor interface is given by:

$$v_i = - \left[\frac{C \mu_\infty \Delta W \xi'}{x^{1/4} \rho Sc (1 - W)} \right]_i \quad (85)$$

Aerosol fluxes estimated on the basis of (85) were compared to those calculated from equation (68). This comparison, presented as the ratio of calculated to estimated values in Table VII, shows the agreement to be fairly good for conditions of large particle sizes and rapid condensation rates. For smaller particles and lower condensation rates, the influence of Brownian diffusion becomes significant, causing the calculated deposition rates to deviate significantly from those that were estimated on the basis of equation (85).

In all of the cases studied, the neglect of thermophoresis and the diffusio-phoretic correction factor caused the approximation to predict deposition rates lower than those calculated from the boundary-layer analysis. An additional factor that caused the estimated results to fall below those of the boundary-layer analysis was the assumption of one-dimensional behavior, which precluded the assessment of particle transport arising from the longitudinal component of velocity.

TABLE VII
COMPARISON OF COMPUTED AND ESTIMATED
DEPOSITION RATES

<u>Run</u>	$\frac{\dot{m}_a \times 1/4 \text{ Computed}}{\dot{m}_a \times 1/4 \text{ Estimated}}$
1-1-.01	2.59
1-4-.01	1.27
1-16-.01	1.24
1-1-.05	1.44
1-4-.05	1.29
1-16-.05	1.29
1-1-.1	1.56
1-4-.1	1.54
1-16-.1	1.54

Relative Contributions to Particle Transport by Individual Mechanisms

To conclude the foregoing discussion of the computed results, it is appropriate to examine the individual mechanisms of particle transport in terms of their separate contributions to the total deposition process. Brownian diffusion is of particular importance in this respect, since it is the only mechanism which depends strongly on particle size -- a property which is

significant whenever heterogeneous aerosols are present. The aerosol fluxes given in Table IV show a decreasing dependency on particle size as particle size increases (diffusion coefficient decreases). For even larger particle sizes, the results indicate that a limiting deposition rate is approached, which apparently depends solely on the diffusiophoretic, thermophoretic, and flow properties of the fluid.

Such behavior can be visualized further by considering the peculiar interaction of the Brownian diffusion process with other mechanisms of transport. Diffusiophoresis and thermophoresis supply an influx of particles that force a concentration gradient to become established which, in accordance with the associated diffusion coefficient, will account for deposition at the prescribed rate. From such behavior, one can assess the effect of small perturbations in flow structure within the boundary layer. The resulting increase in the apparent particle diffusivity will obviously affect the shape of the particle concentration-profile. This change, however, will tend to occur in a manner so as to accommodate the influx of particles, resulting in only a minor change of the gross deposition rate.

In this context, the range of particle sizes chosen for study in the present investigation should be mentioned. On the basis of previous studies[7], this range was thought to fall on the lower portion of the expected spectrum of particle sizes. Subsequent analyses, however, have indicated that the sizes of aerosol particles existing under post-accident conditions may be larger than expected previously. Regardless of this, the relative independence of deposition rates on particle size renders these considerations of minor importance so far as gross rates of particle transport are concerned.

In preliminary computations performed during this investigation, particle transport rates were calculated assuming the thermophoretic effect to be negligible. These results may be compared with those given in Table IV, to assess the individual contribution of thermophoresis to the overall deposition process. This comparison is shown in Table VIII, where the ratio of particle-deposition rates, including and excluding thermophoresis, is given for each of the runs.

The relative effect of the diffusiophoretic correction factor is also of interest. Although this cannot be evaluated directly on the basis of results obtained in the present study, some idea of its effect can be obtained by comparison of the individual velocity contributions in equation (9). Table IX

TABLE VIII

EFFECT OF THERMOPHORESIS ON AEROSOL DEPOSITION RATES

<u>Run</u>	<u>Ratios of Deposition Rates</u> <u>[Including Thermophoresis]</u> <u>[Neglecting Thermophoresis]</u>
1-1-.01	1.01
1-1-.05	1.03
1-1-.1	1.09
1-4-.01	1.04
1-4-.05	1.08
1-4-.1	1.09
1-16-.01	1.07
1-16-.05	1.08
1-16-.1	1.08

TABLE IX

ESTIMATED EFFECTS OF THE DIFFUSIOPHORETIC CORRECTION FACTOR

<u>Run</u>	<u>Particle Flux Ratio</u> <u>[Flux from Equation (10)]</u> <u>[Computed Flux (Table IV)]</u>
1-1-.01	.017
1-1-.05	.034
1-1-.1	.034
1-4-.01	.031
1-4-.05	.034
1-4-.1	.034
1-16-.01	.032
1-16-.05	.032
1-16-.1	.032

gives one such comparison, presenting the ratios of total particle fluxes to those attributed to the diffusio-phoretic correction factor alone. Here total particle fluxes were taken from Table IV. Fluxes corresponding to the diffusio-phoretic correction factor were estimated on the basis of equation (10), assuming unit γ at the liquid-vapor interface. Because of the neglect of axial contributions, the estimated effects of the diffusio-phoretic correction factor given in Table IX are expected to be somewhat lower than those encountered in practice.

From the foregoing analysis, one may conclude that of all the mechanisms of particle transport, diffusio-phoresis is of primary importance in determining deposition rate. Particle diffusion is important in establishing concentration profiles, but is of minor importance in determining deposition rates, except for cases where particle size is extremely small. Effects of the diffusio-phoretic correction factor and thermophoresis are of secondary importance, each accounting for less than 10 percent of the total effect under the most extreme conditions studied.

APPLICATION TO REAL SYSTEMS

In applying results of the boundary-layer analysis, one must examine the significance of its idealities in light of real-system characteristics. The characteristics of real systems are diverse, and cannot be considered in detail here. Instead, the results will be applied for an extremely simple macroscopic system, with a subsequent discussion of ramifications arising when more complex conditions are encountered. Such a discussion should form a basis for further applications to individual systems, and provide an idea of the conditions under which such applications are appropriate.

Such a system is shown in Figure 18. It consists of a right, circular cylinder of length h and radius r . In accordance with the previous derivations, we assume constant bulk, wall, and interface temperature, and laminar behavior. Total aerosol, steam, and energy transport may be obtained by integrating equations (66), (67), and (68) over the vertical wall, hence,

$$w_{\text{aerosol}} = 2\pi r \cdot \frac{4 h^{3/4}}{3} \left[\frac{C_{\beta} N^i}{\phi^2} \right]_i \frac{\text{particles}}{\text{unit time}} \quad (86)$$

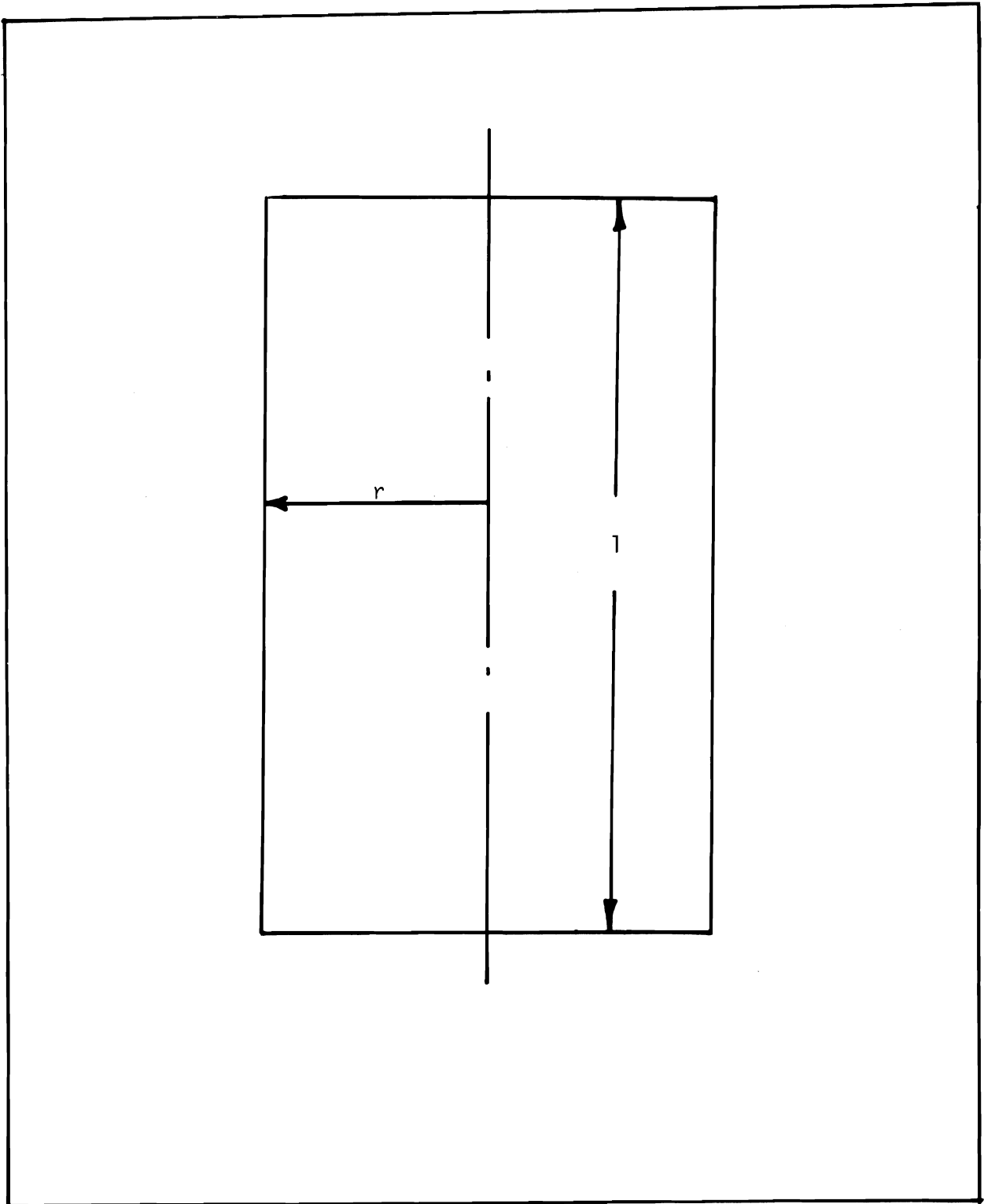


FIGURE 18

SCHEMATIC OF SIMPLIFIED VESSEL

$$w_{\text{steam}} = 2\pi r \cdot \frac{4 h^{3/4}}{3} \frac{C \mu_{\infty} \xi^i (\Delta W)}{(1 - W) Sc} \Big|_i \frac{\text{mass}}{\text{unit time}}, \quad (87)$$

and

$$Q = 2\pi r \cdot \frac{4 h^{3/4}}{3} \frac{C C_p \mu_{\infty} \Delta T}{Pr_{\infty}} + \frac{\lambda \mu_{\infty} \Delta W \xi^i}{Sc (1 - W)} \Big|_i \frac{\text{energy}}{\text{unit time}}. \quad (88)$$

For an example, we apply these equations to a vessel wherein $h = 40$ ft. and $r = 10$ ft. For conditions similar to those of run 1-1, wherein the aerosol loading consists of 10^7 0.1 micron particles per cubic foot, these give

$$w_{\text{aerosol}} = 2.63 \times 10^9 \frac{\text{particles}}{\text{hour}}, \quad (89)$$

$$w_{\text{steam}} = 23.7 \frac{\text{pounds}}{\text{hour}}, \quad (90)$$

$$Q = 2.37 \times 10^4 \frac{\text{BTU}}{\text{hour}}. \quad (91)$$

Performing total material and energy balances for the system of $\pi r^2 h$ ft³ volume, equations (89) and (90) lead to predicted instantaneous aerosol and steam decay rates of 2.1 and 5.0%/hour, respectively. The corresponding rate of temperature fall is about 3°F/hr.

Several criticisms of this application might be voiced. Among these are:

1. Transfer to the vessel ends has been neglected.
2. Perturbations of the boundary layer arising from the closed ends have been assumed unimportant.
3. Upwelling of the fluid in the center of the vessel is assumed to have negligible effect on material and energy fluxes.
4. The possibility of transition to a turbulent boundary layer is neglected.
5. Any nonuniformity in interface and bulk properties is assumed to be negligible.
6. Any subsaturation of the bulk mixture is taken to be negligible.
7. Transient effects are neglected through assumption of a quasi-steady state.

Most of these criticisms are not serious. Transfer to the ends of the vessel can be estimated roughly by assuming its effect to be proportional to

the ratio of head area to total area. Because of the large ratio between vessel height and boundary-layer width, end effects are expected to be negligible. Upward fluid velocity is small in most cases^[9], and the effect of axial velocity on radial heat and mass transport is of secondary importance, anyway. The assumption of constant surface and bulk properties has been shown to be reasonably valid in several containment experiments^[9]; and subsaturation, although it undoubtedly does tend to occur, is negligible for all practical purposes.

The assumption of a quasi-steady state implies that the time-rate of accumulation within the boundary layer is small compared to rates of gross transport -- a condition that undoubtedly is met for all systems of reasonably large size. Applicability of the quasi-steady state assumption allows transient response to be predicted simply in a totally satisfactory manner. This is accomplished by combining wall transport rates with total system balances, and stepping off in incremental elements of time.

Neglect of turbulent transport is undoubtedly the most serious of all the criticisms listed. For energy and steam transport, where molecular diffusivities are relatively high, this problem can be circumvented by using the previously mentioned empirical correlations and analogies.^[8] Because of fundamental differences in transport mechanisms, however, such analogies cannot be applied to determine particle transport rates in turbulent boundary layers. Provided that particle transport rates in the turbulent boundary layer are known, they can be combined with those for the laminar boundary layer using standard methods, and composite behavior can be defined. In this respect, a large portion of the applicability of the present work will be realized only after further work is accomplished in analyzing turbulent deposition. Theoretical and experimental work regarding mechanisms of deposition in turbulent boundary layers is practically nonexistent at the present time. Accordingly, acquisition of such information would significantly increase the level of understanding of natural-process removal.

Further complexities in the macroscopic system, such as internal structures, transient sources, and nonideal geometries, will obviously complicate natural-response analysis. Here, the judgment of the person performing the analysis is of great importance to its success. In the event that proper judgment is exercised, however, the results presented in the previous sections should be useful to the basic analysis.

CONCLUSIONS

1. Boundary layer equations have been formulated and solved which describe aerosol transport in a laminar condensing-steam system. These solutions are presented as profiles of velocity, steam concentration, aerosol concentration, and temperature. From the solutions one may compute wall fluxes for use in analyzing the transient response of post-accident containment systems.
2. For steam-air mixtures adjacent to a vertical wall, laminar and turbulent boundary-layer flow regimes occur under the following conditions:

$$\text{laminar} \leftarrow 1.5 \times 10^8 < \overset{\text{transitional}}{\text{Gr}} > 1.5 \times 10^{10} \rightarrow \text{turbulent.}$$

3. Approximate particle-deposition trajectories have been computed. These indicate that a large portion of particles entering the laminar boundary layer will deposit down-wall, where turbulent or transitional conditions exist.
4. There is a tendency for the boundary-layer region to become subsaturated. This will result in a similar tendency for the bulk mixture to become subsaturated, owing to the simultaneous heat-transfer - mass-transfer process. This implies that other types of heat sinks, such as cold sprays, also will tend to cause subsaturation of the bulk mixture.
5. Use of the heat-transfer - mass-transfer analogy in conjunction with experimental heat-transfer data is an accurate means for estimating condensation rates in laminar boundary layers. Such an analogy is probably valid for turbulent boundary layers as well.
6. Diffusiophoresis is the predominant factor in controlling aerosol deposition rates. Both thermophoresis and the diffusiophoretic correction term are responsible for only about 10% of the total deposition rate, even under the most extreme circumstances studied. Brownian diffusion does not influence the rate of particle deposition except for conditions where very low condensation rates and fine particle sizes are encountered.
7. An approximate, one-dimensional analysis, which assumes particles to be deposited with the mass-average velocity of the fluid, has been compared with the computed results. This analysis gives deposition rates that are from 20% to 60% lower than those predicted from the boundary-layer theory, depending upon physical conditions of the system.

REFERENCES

- [1] R.B. Bird, W.E. Stewart, and E.N. Lightfoot. Transport Phenomena, John Wiley & Sons, Inc., New York, New York, pp 84, 318, 514, and 559, (1960).
- [2] B. Carnahan, H.A. Luther, and J.O. Wilkes. Applied Numerical Methods, John Wiley & Sons, Inc., New York, New York, in press.
- [3] R. Cheesewright. "Turbulent Natural Convection from a Vertical Plane Surface," Journal of Heat Transfer, Vol. 90, pp 1-7, (1968).
- [4] E.R.G. Eckert. Introduction to Heat and Mass Transfer, McGraw-Hill, Inc., New York, New York, p. 186, (1963).
- [5] A. Einstein. Investigations on the Theory of Brownian Movement, Dover, Inc., U.S.A., p. 11, (1956).
- [6] J.D. Hellums, and S.W. Churchill. "Simplification of the Mathematical Description of Boundary and Initial Value Problems," A.I.Ch.E. Journal, Vol. 10, pp 110-114, (1964).
- [7] R.K. Hilliard, L.F. Coleman, J.D. McCormack. Comparisons of the Containment Behavior of a Simulant with Fission Products Released from Irradiated UO₂, BNWL-581, Pacific Northwest Laboratory, Richland, Washington, March, 1968.
- [8] T.W. Horst. A Review of Particle Transport in a Condensing Steam Environment, BNWL-848, Pacific Northwest Laboratory, June, 1968.
- [9] J.G. Knudsen and R.K. Hilliard. Fission Product Transport by Natural Processes in Containment Vessels, BNWL-943, Pacific Northwest Laboratory, January, 1969.
- [10] W.J. Minkowycz. Laminar Film Condensation of Water Vapor on an Isothermal Vertical Surface, Ph.D. Thesis in Mechanical Engineering, University of Minnesota, 1965.
- [11] W.J. Minkowycz, and E.M. Sparrow. "Condensation Heat Transfer in the Presence of Noncondensables, Interfacial Resistance, Superheating, Variable Properties, and Diffusion," Intern. J. Heat and Mass Transfer, Vol. 9, pp 1125-1144, (1966).
- [12] W. Nusselt. Z. Ver. deut. Ing., Vol. 60, pp 541-569, (1916).
- [13] M.N. Ozisik, and D. Hughes. "Effects of Natural Convection on Removal of Fission Products from Steam-Air Mixtures," Paper presented at 1969 Annual Meeting of the American Nuclear Society, June 15-19, 1969.
- [14] R.C. Reid, and T.K. Sherwood. The Properties of Gases and Liquids, McGraw-Hill, Inc., New York, New York, (1958).
- [15] H. Schlichting. Boundary Layer Theory, McGraw-Hill, Inc., New York, New York, p. 334, (1962).

- [16] E.M. Sparrow and S.H. Lin. "Condensation Heat Transfer in the Presence of a Non-Condensable Gas," Journal of Heat Transfer, Vol. 86, pp 430-436, (1964).
- [17] L. Waldmann. "Über die Kraft eines Inhomogenen Gases auf Kleine Suspendierte Kugeln," Z. Naturforsch, Vol. 14a, pp 589-599, (1959).

TABLE OF NOMENCLATURE

a	=	Constant defined by equation (46).
b	=	Constant defined by equation (47).
c	=	Concentration, lb-moles/ft ³ .
C	=	Constant defined by equation (27).
C _p	=	Specific heat of gas mixture, BTU/lbm °F.
C _{pa}	=	Specific heat of air, BTU/lbm °F.
C _{pw}	=	Specific heat of steam, BTU/lbm °F.
D	=	Aerosol diffusion coefficient, ft ² /hr.
D _{AB}	=	Air-steam diffusion coefficient, ft ² /hr.
F	=	Dimensionless variable defined by equation (25).
g	=	Gravitational acceleration, ft/hr ² .
Gr	=	Grashoff Number, defined by equation (2).
h	=	Height of test vessel, feet, also heat-transfer coefficient, BTU/ft ² hr °F.
k	=	Thermal conductivity, BTU/ft hr °F.
k _x	=	Mass transfer coefficient, lb-moles/hr ft ² .
L	=	Distance down wall, feet.
\dot{m}_h	=	Interfacial flux of energy away from wall, BTU/ft ² hr.
\dot{m}_h'	=	Interfacial flux of energy through gaseous boundary layer by conduction, BTU/ft ² hr.
\dot{m}_p	=	Interfacial flux of aerosol particles away from wall, particles/ft ² hr.
\dot{m}_w	=	Interfacial flux of steam away from wall, lbm/ft ² hr.
M	=	Molecular weight.
N	=	Aerosol particle concentration, particles/ft ³ .
Nu	=	Nusselt number, (local) hL/k.
P	=	Total pressure, lbf/ft ² .
Pr	=	Prandtl Number.
q	=	Constant defined by equation (44).
q _t	=	Interfacial flux of energy away from wall, BTU/ft ² hr. q _t = \dot{m}_h .
r	=	Radius of test vessel, feet.
Sc	=	Schmidt Number, D _{AB} /ν.
Sh	=	Sherwood Number, (local) k _x L/c D _{AB} .
T	=	Temperature, °F.
u	=	Down-plate mass-average velocity, ft/hr.
v	=	Outward, normal mass-average velocity, ft/hr.
W	=	Mass fraction of steam.

- w = Deposition rate, lb/hr, or particles/hr.
 x, y = Distance variables defined in Figure 1.
 β = Constant defined by equation (43).
 δ = Liquid-film thickness, feet.
 Δ = Operator denoting the difference between bulk and interfacial conditions.
 η = Transformation variable defined by equation (26).
 λ = Latent heat of vaporization of water, BTU/lbm.
 μ = Dynamic viscosity, lbm/ft hr.
 ν = Kinematic viscosity, ft²/hr.
 ξ = Normalized mass fraction of water, $(W-W_i)/(W_\infty-W_i)$.
 π = Density ratio, ρ_∞/ρ .
 ρ = Density, lbm/ft³.
 Σ_1, Σ_2 = Variables defined by equations (40) and (41).
 τ = Normalized temperature, $(T-T_i)/(T_\infty-T_i)$.
 ϕ_C = Specific heat ratio, $C_p/C_{p\infty}$.
 ϕ_{Cvg} = Specific heat difference, $(C_{pw}-C_{pa})/C_{p\infty}$.
 ϕ_μ = Viscosity ratio, μ/μ_∞ .
 ψ = Stream function defined by equations (24a, b).
 \mathbb{T} = Normalized particle concentration, $(N-N_i)/(N_\infty-N_i)$.

Subscripts

- a = Air
 c = Diffusiophoretic correction
 G = Gas
 i = Interface
 L = Liquid
 P = Aerosol particle
 t = Thermophoresis
 w = Water

APPENDIX 1

COMPUTER NETWORK AND DIFFERENCE EQUATIONS

Finite-Difference Approximations to the Particle-Transport Equation

The finite-difference approximations used for solution of equation (39) were written with respect to the increment spacing shown in Figure A-1.

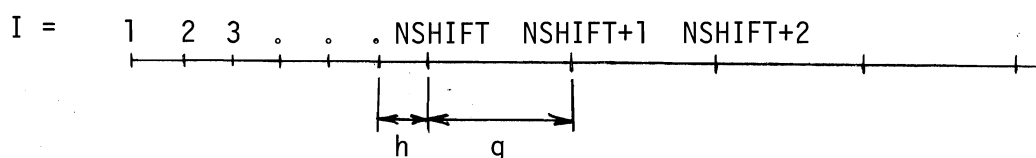


FIGURE A-1

INCREMENT SPACING FOR FINITE DIFFERENCE APPROXIMATIONS

These are:

$$\tau(n - h) A(I) + \tau(n) B(I) + \tau(n + h) C(I) = 0 \quad (A-1)$$

for $I < NSHIFT$,

$$\tau(n - g) A(I) + \tau(n) B(I) + \tau(n + g) C(I) = 0 \quad (A-2)$$

for $I > NSHIFT$, and

$$\tau(n - h) A(I) + \tau(n) B(I) + \tau(n + g) C(I) = 0 \quad (A-3)$$

for $I = NSHIFT$, where $NSHIFT$ is the index where grid enlargement takes place.

The coefficients in equations (A-1) through (A-3) are given as follows:
For $1 < I < NSHIFT$ and $NSHIFT < I < N$,

$$A(I) = \left(-\frac{L}{(\Delta\eta)^2} - \frac{\Sigma_1(I)}{2\Delta\eta} \right) \quad (A-4)$$

$$B(I) = \left(\frac{2L}{(\Delta\eta)^2} + \Sigma_2(I) \right), \quad (A-5)$$

and

$$C(I) = \left(-\frac{L}{(\Delta\eta)^2} + \frac{\Sigma_1(I)}{2\Delta\eta} \right), \quad (A-6)$$

where $L = \beta Sc/v_\infty$, and N is the uppermost index of I . Here $\Delta\eta = h$ for $1 < I < \text{NSHIFT}$, and $\Delta\eta = g$ for $\text{NSHIFT} < I < N$. For $I = \text{NSHIFT}$ the coefficients are given by:

$$A(I) = - \frac{L(h - g)}{h(g^2 + h^2)} - \frac{2L}{g^2 + h^2} - \frac{\Sigma_1(I)}{2h}, \quad (\text{A-7})$$

$$B(I) = \frac{L(h - g)}{g^2 + h^2} \left(\frac{1}{h} - \frac{1}{g} \right) - \frac{4L}{g^2 + h^2} + \frac{\Sigma_1(I)}{2} \left(\frac{1}{g} - \frac{1}{h} \right) - \Sigma_2(I), \quad (\text{A-8})$$








and

$$C(I) = \frac{L(h - g)}{h(g^2 + h^2)} + \frac{2L}{g^2 + h^2} - \frac{\Sigma_1(I)}{2g}. \quad (\text{A-9})$$

The finite-difference equations were solved by expressing them and their boundary conditions in terms of a tridiagonal matrix, which was solved in turn to obtain the corresponding epsilon values.

Schematic Analog Network

The Analog-Computer network used for solution of the boundary layer problem is shown in Figure A-2. The symbolism is defined as follows:

-  = potentiometer
-  = linear amplifier
-  = high-gain amplifier
-  = integrator
-  = multiplier
-  = divider
-  = trunk line to (or from) digital computer.

Scale Factors for Analog Solutions

Table A-1 gives scale factors used for each of the analog-computer runs. Scale factor is defined as an absolute value of the number that, when multiplied by the value of the computed variable, will give the analog-computer voltage corresponding to that variable. The letters given in Table A-1 correspond to those shown in the network in Figure A-2.

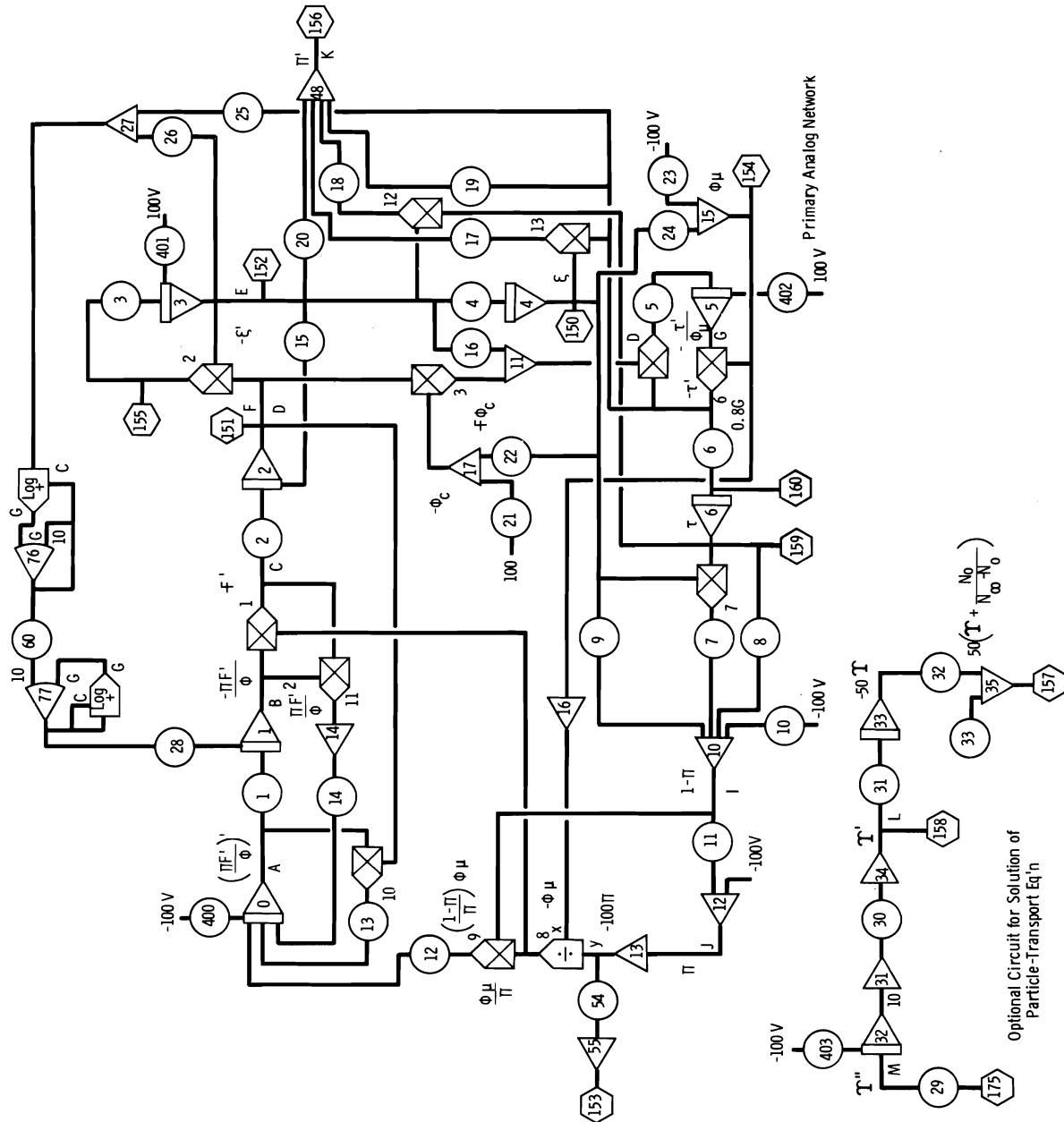


FIGURE A2

ANALOG-COMPUTER NETWORK

TABLE A-1
SCALE FACTORS FOR ANALOG-COMPUTER SOLUTIONS

<u>Run</u>	<u>Scale Factors</u>						
	<u>A</u>	<u>B</u>	<u>D</u>	<u>E</u>	<u>G</u>	<u>I</u>	<u>K</u>
0.5-1	7000	3333	400	500	500	20,000	100,000
0.5-2	3000	2500	400	500	400	10,000	40,000
0.5-4	2000	2000	300	400	350	5,000	15,000
0.5-8	1000	1300	250	300	250	2,500	7,000
0.5-16	600	1000	250	300	250	1,400	3,000
1-1	5000	3333	400	500	500	15,000	80,000
1-2	3000	2500	400	500	400	7,500	30,000
1-4	2000	2000	300	400	350	5,000	15,000
1-8	1000	1300	250	300	250	2,000	5,000
1-16	600	1000	200	300	250	1,100	2,000
2-1	5000	3333	400	500	500	10,000	50,000
2-2	3000	2500	400	500	400	7,000	20,000
2-4	2000	2000	300	400	350	3,500	10,000
2-8	1000	1300	250	300	250	1,800	4,000
2-16	600	1000	200	250	200	1,000	2,000

APPENDIX 2

TABULATED VALUES OF Σ_1 AND Σ_2

Values of Σ_1 and Σ_2 were taken from the hybrid-computer output and interpolated to correspond to common values of η . The interpolant values are given in Table A-II. Values of Σ_1 do not include the factor

$$\frac{2 \beta Sc \phi_{\mu}'}{v_{\infty} \phi_{\mu}},$$

because of its dependence on particle characteristics. This factor is so small that it does not affect the values of Σ_1 significantly, and can be ignored for all practical purposes.

One should note that the six-place decimals in the computer output do not imply that the results are this accurate. Error estimates for the tabulated values are given in the DISCUSSION OF RESULTS section of the main report.

TABLE A-2
SUMMARY OF HYBRID-COMPUTER OUTPUT

Part I -- 0.5 Atm. Steam

- 1000 Σ_2

- Σ_1

ETA	.5-1	.5-2	.5-4	.5-8	.5-16	.5-1	.5-2	.5-4	.5-8	.5-16
0.00	.001037	.002648	.005962	.013286	.029565	.000299	.000956	.004795	.022192	.100515
1.00	.010254	.017276	.029129	.052273	.090673	.001959	.008171	.029476	.130054	.438371
2.00	.032733	.053889	.084034	.132549	.209777	.007270	.026130	.097057	.334676	1.082826
3.00	.062263	.093266	.147999	.220865	.327327	.014020	.045716	.152442	.468145	1.329722
4.00	.094803	.143677	.208793	.296357	.413646	.019354	.061118	.182556	.481429	1.171138
5.00	.127845	.185442	.261283	.354869	.474839	.022252	.066277	.177161	.414297	.851066
6.00	.166775	.221622	.302363	.394896	.512609	.023162	.063677	.148747	.318321	.545780
7.00	.182800	.251141	.333209	.420878	.536615	.022769	.057635	.121891	.210290	.339701
8.00	.204382	.274290	.355657	.437124	.552266	.020483	.046541	.088510	.146931	.188809
9.00	.222256	.291859	.371121	.446364	.562916	.017926	.036520	.061949	.101381	.088811
10.00	.236291	.305068	.382514	.452042	.570258	.014702	.027584	.043083	.052940	.062702
11.00	.247220	.315014	.390214	.454445	.575877	.012102	.021345	.030691	.031876	.045149
12.00	.255413	.322268	.395917	.455007	.580135	.009426	.015909	.021705	.027102	.021625
13.00	.261673	.327752	.399690	.454901	.583773	.007372	.011218	.016375	.021195	.015831
14.00	.266370	.331802	.402530	.454700	.587099	.005599	.008089	.011092	.015222	.012860
15.00	.269745	.334779	.403621	.454863	.590117	.004200	.005593	.006173	.012905	.010088
16.00	.272083	.337024	.406332			.003412	.004245	.004625		
17.00	.273734	.338836	.407657			.002777	.003354	.003825		
18.00	.274853	.340367	.408775			.002222	.002628	.002924		
19.00	.275538	.341670	.409633			.001801	.002009	.002145		
20.00	.275799	.342692	.410968			.001585	.001577	.001589		

TABLE A-2 (Continued)

SUMMARY OF HYBRID-COMPUTER OUTPUT

Part II -- 1 Atm. Steam

ETA	- Σ_1										- 1000 Σ_2			
	1-1	1-2	1-4	1-8	1-16	1-1	1-2	1-4	1-8	1-16	1-1	1-2	1-4	1-8
0.00	.601832	.004273	.010201	.023629	.053319	.000808	.002370	.012075	.061069	.308677				
1.00	.012660	.022124	.036619	.071643	.129547	.003538	.013966	.055349	.227175	.960668				
2.00	.039465	.062658	.103827	.164568	.263742	.011729	.042261	.161233	.541206	1.793716				
3.00	.074138	.113598	.175733	.262686	.384578	.021259	.071127	.233047	.710400	1.884436				
4.00	.110443	.163287	.240875	.340672	.467078	.028954	.090158	.261283	.676219	1.438774				
5.00	.145988	.209923	.295725	.399230	.519527	.032342	.092567	.243740	.540821	.936130				
6.00	.177900	.246381	.336624	.433369	.549559	.032549	.084519	.195242	.394152	.581393				
7.00	.204828	.276708	.366276	.463451	.565972	.031092	.072524	.153223	.266152	.339529				
8.00	.227330	.293316	.386618	.479104	.574412	.027222	.057622	.110645	.166478	.174416				
9.00	.245408	.316548	.400533	.483746	.578632	.023141	.045071	.076716	.101087	.078388				
10.00	.259357	.323803	.410141	.494516	.580312	.018537	.033406	.049470	.063426	.058752				
11.00	.270172	.337912	.416144	.498127	.581069	.014601	.023958	.032751	.041181	.047112				
12.00	.278527	.344400	.420201	.500257	.581061	.011472	.017246	.021930	.025319	.020285				
13.00	.284822	.349126	.422841	.501647	.580999	.008920	.011960	.014430	.017972	.010443				
14.00	.289661	.352459	.424541	.502536	.581032	.007006	.009025	.010077	.012766	.004743				
15.00	.293301	.354800	.425530	.502749	.580985	.005275	.006703	.007773	.009144	.001767				
16.00	.295950	.356463	.426001			.003964	.005092	.006441						
17.00	.297944	.357605	.426208			.003020	.003817	.004228						
18.00	.299356	.358406	.426224			.002455	.002818	.002641						
19.00	.300403	.358999	.426036			.001889	.001841	.001780						
20.00	.301227	.359476	.425536			.000939	.001206	.002152						

TABLE A-2 (Continued)

SUMMARY OF HYBRID-COMPUTER OUTPUT

Part III -- 2 Atm. Steam

ETA	- Σ_1					- 1000 Σ_2				
	2-1	2-2	2-4	2-8	2-16	2-1	2-2	2-4	2-8	2-16
1.00	.003279	.007753	.014029	.041722	.094049	.001262	.005644	.027519	.140414	.655514
1.00	.016276	.020930	.052815	.098869	.182982	.005207	.021701	.086397	.386672	1.499214
2.00	.046482	.075110	.123397	.204574	.328279	.015541	.058078	.223250	.758683	2.412593
3.00	.084769	.131603	.202909	.306750	.445927	.027256	.091535	.304423	.903121	2.315450
4.00	.123274	.185506	.270978	.385839	.523332	.036433	.113458	.322383	.822066	1.679042
5.00	.163385	.233378	.326654	.443023	.570201	.040798	.115140	.292074	.630941	.999125
6.00	.196008	.272212	.366329	.480228	.595336	.040483	.101616	.225798	.424553	.598528
7.00	.223511	.302767	.394471	.503645	.609204	.037616	.084715	.170597	.270762	.329805
8.00	.245745	.320758	.412762	.518007	.616761	.031606	.066205	.110497	.165242	.170377
9.00	.262784	.340900	.424974	.526700	.621048	.026224	.051971	.079845	.097831	.116120
10.00	.275799	.352654	.432530	.531793	.623144	.020954	.038200	.051237	.062502	.056296
11.00	.285343	.360496	.437125	.534794	.624403	.016417	.025721	.035233	.042205	.026350
12.00	.292279	.366242	.440162	.535842	.625501	.012705	.018739	.024534	.024421	.010310
13.00	.297128	.370079	.441635	.535966	.626554	.009784	.013264	.015943	.016145	.007180
14.00	.300432	.373006	.442000	.535808	.627550	.007297	.009047	.011882	.011315	.006787
15.00	.302562	.374878	.441981	.535995	.628001	.005376	.005435	.009072	.007489	.000521
16.00	.303852	.375728	.441994			.004223	.003706	.007125		
17.00	.304599	.376327	.441973			.003237	.003050	.006669		
18.00	.304980	.376771	.441996			.002508	.002420	.002790		
19.00	.305090	.377052	.442042			.001991	.001825	.001600		
20.00	.304963	.376913	.442000			.001646	.001801	.001325		

APPENDIX 3

PHYSICAL PROPERTIES

Physical properties of steam-air mixtures were obtained through combination of the pure component properties using recommended methods. The sources and combination methods are listed as follows:

Saturation conditions -- Taken from steam data given in the Electrical Research Association 1967 Steam Tables, Thomas Nelson, Ltd., Edinburgh, (1967). Dalton's law and the ideal-gas relationship were utilized for determining mixture properties.

Viscosity values -- Taken from NBS - NACA Tables of Thermal Properties of Gases. Mixture properties estimated by the Wilke method, as described in R.C. Reid and T.K. Sherwood, The Properties of Gases and Liquids, McGraw-Hill, Inc., New York, New York, p. 199 (1958). (Hereafter referred to as R&S).

Specific-heat values -- Taken from NBS-NACA Tables of Thermal Properties of Gases. Mixture properties estimated by weighting individual properties with the corresponding mass fraction.

Thermal-conductivity values -- Taken from NBS-NACA Tables of Thermal Properties of Gases. Mixture properties estimated by method of Lindsay and Bromley as described in R&S, p. 240.

Mutual-diffusion-coefficient values -- Taken from physical data interpolated by E.A. Mason and L. Monchick, "Survey of The Equation of State and Transport Properties of Moist Gases," 1963 International Symposium on Humidity and Moisture, National Bureau of Standards, Washington, D.C., (1963).

Aerosol diffusion-coefficient values -- Calculated from the (corrected) relationship given by C.N. Davies, Aerosol Science, Academic Press, New York, New York, p. 408, (1966).

Physical properties estimated by these methods are listed in Tables A-3 and A-4.

TABLE A-3

ESTIMATED STEAM-AIR PROPERTIES (SATURATED STEAM)

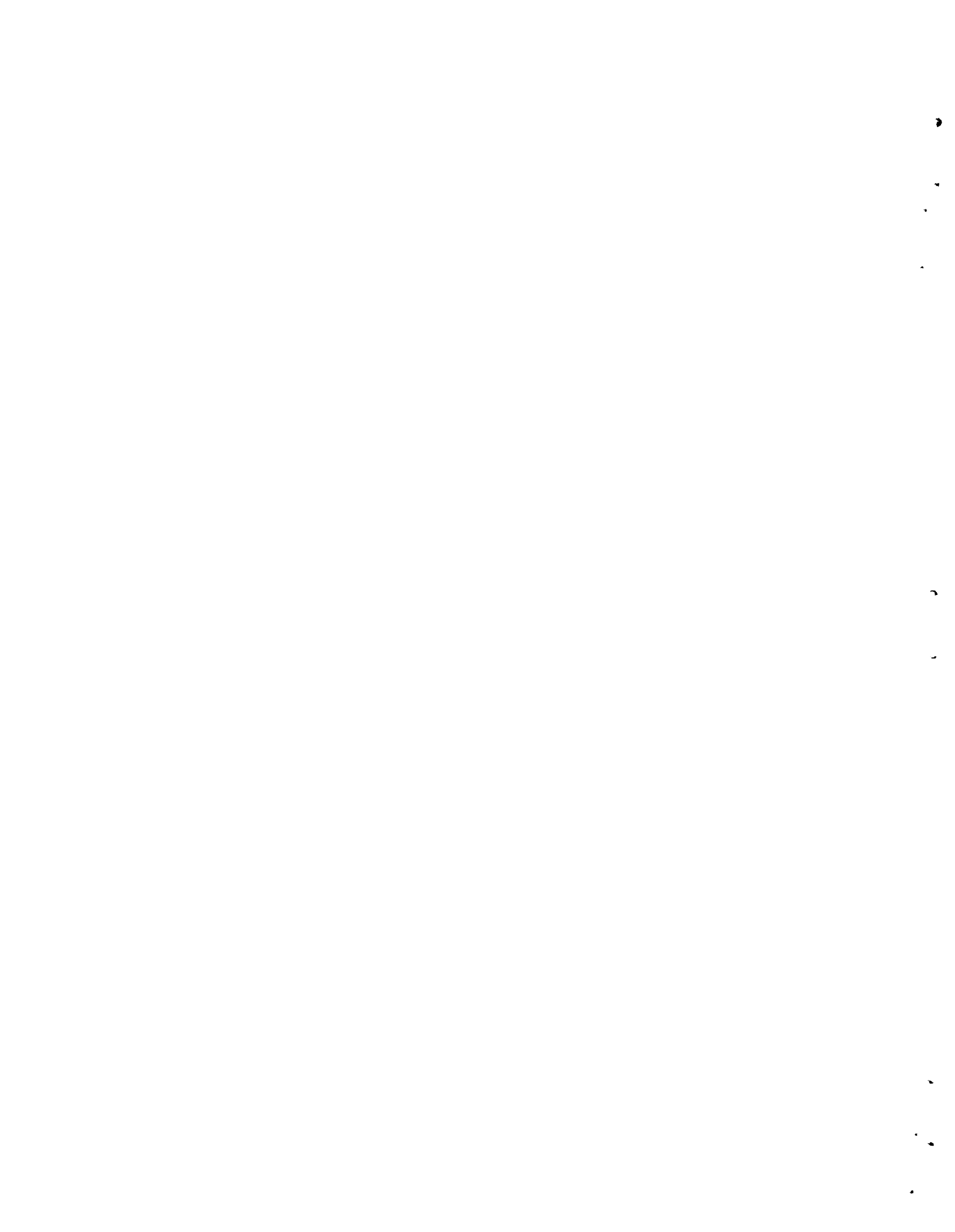
T °R	P _{air} lbf/ft ²	P _{steam} lbf/ft ²	W	μ lbm/ft hr	ν ft ² /hr	DAB ft ² /hr	k BTU/ft hr °F	Cp BTU/lbm °F	Pr	Sc
708.7	2779	4220	.48570	.0403	.279	.124	.0179	.374	.839	.580
707.7	2852	4146	.47480	.0405	.278	.124	.0180	.371		.578
706.7	2925	4074	.46415	.0406	.277	.124	.0180	.367		.577
704.7	3067	3932	.44365	.0410	.276	.123	.0180	.362		.580
700.7	3338	3661	.40545	.0417	.275	.122	.0181	.350		.581
692.7	3835	3164	.33905	.0429	.272	.120	.0182	.332		.584
671.7	2634	2116	.33318	.0419	.378	.170	.0176	.325	.774	.574
670.7	2676	2075	.32583	.0421	.378	.170	.0176	.323		.573
669.7	2716	2034	.31768	.0422	.377	.169	.0177	.321		.575
667.7	2796	1954	.30290	.0425	.375	.168	.0176	.317		.577
663.7	2948	1802	.27538	.0430	.373	.166	.0176	.309		.579
655.7	3223	1530	.22760	.0439	.367	.164	.0176	.297		.578
638.7	2504	1059	.20804	.0436	.468	.209	.0173	.290	.731	.578
637.7	2528	1035	.20289	.0436	.467	.209	.0173	.289		.577
636.7	2551	1012	.19786	.0437	.466	.208	.0173	.288		.578
634.7	2595	967	.18816	.0439	.464	.208	.0173	.285		.579
630.7	2679	883	.17010	.0442	.460	.207	.0172	.281		.579
622.7	2829	733	.13879	.0448	.452	.205	.0171	.273		.580

TABLE A-4

VALUES OF β USED FOR CALCULATION*

<u>RUN</u>	<u>β ft²/hr</u>
1-1-.01	0.00127
1-4-.01	0.00126
1-16-.01	0.00125
1-1-.05	0.0000651
1-4-.05	0.0000650
1-16-.05	0.0000643
1-1-.1	0.0000217
1-4-.1	0.0000216
1-16-.1	0.0000214

* Defined as $\beta = (D\phi_{\mu})_{avg}$, where $(D\phi_{\mu})_{avg} = \frac{D_{\infty} + (D\phi_{\mu})_i}{2}$.



DISTRIBUTION

No. of
Copies

- 1 AEC, Chicago Operations Office
9800 South Cass Avenue
Argonne, Illinois 60439
G.H. Lee, Director, Patent Division
- 2 AEC, Chicago Patent Group
Federal Bldg., 700 Area
Richland, Washington 99352
R.K. Sharp
- 8 AEC Library, Washington, D.C. 20545
Division of Reactor Development & Technology
A.J. Pressesky, Assistant Director Safety (5)
H.L. Hamester
I.C. Roberts
S.A. Szawlewicz
- 5 AEC Division of Technical Information Extension
P.O. Box E
Oak Ridge, Tennessee
- 1 Assistant Director for Pacific Northwest Programs, DRDT
P.O. Box 550
Richland, Washington 99352
T.A. Nemzek/P.G. Holsted
- 2 AEC Richland Operations Office
Federal Bldg., Richland, Washington 99352
C.L. Robinson, Director, Laboratory and University Division
Technical Library
- 3 USAEC, Scientific Representative
c/o Atomic Energy of Canada, Ltd.
Chalk River, Ontario, Canada
R.W. Ramsey
- USAEC/AECL Cooperative Program
TAC and Subcommittees
- 5 Technical Advisory Committee (TAC) - United States
A.N. Tardiff, U.S. Chairman of TAC, AEC Headquarters, Washington, D.C.
20545
H.J. Reynolds U.S. Secretary of TAC, c/o Atomic Energy of Canada, Ltd.,
Sheridan Park, Ontario, Canada
D.F. Babcock, U.S. Member of TAC, E.I. du Pont de Nemours & Co.,
Wilmington, Delaware.
H. Harty, U.S. Member of TAC, Heavy Water Reactor Program Office,
Battelle-Northwest, Richland, Washington 99352

E.A. Mason, U.S. Member of TAC, Massachusetts Institute of Technology, Cambridge, Massachusetts 02139

5 Technical Advisory Committee (TAC) - Canadian

D.D. Stewart, Canadian Chairman of TAC, Atomic Energy of Canada, Ltd., Chalk River Nuclear Laboratories, Chalk River, Ontario, Canada

W.R. Livingston, Canadian Secretary of TAC, Atomic Energy of Canada, Ltd., Chalk River Nuclear Laboratories, Chalk River, Ontario, Canada

L. Pease, Canadian Member of TAC, Atomic Energy of Canada, Ltd. Toronto, Ontario, Canada

R.F.S. Robertson, Canadian Member of TAC, Atomic Energy of Canada, Ltd., Whiteshell Nuclear Research Establishment, Pinawa, Manitoba, Canada.

W.R. Thomas, Canadian Member of TAC, Atomic Energy of Canada, Ltd., Chalk River Nuclear Laboratories, Chalk River, Ontario, Canada

9 TAC Subcommittee - SAFETY

A.J. Pressesky, Nuclear Safety Branch, Division of Reactor Development & Technology, U.S. Atomic Energy Commission, Washington, D.C. 20545

G. Hake, Atomic Energy of Canada, Ltd., Chalk River Nuclear Laboratory, Chalk River, Ontario, Canada

H. Morewitz, Atomics International, P.O. Box 309, Canoga Park, California 91305

R.K. Hilliard, Battelle-Northwest, Richland, Washington 99352

F.C. Boyd, Atomic Energy Control Board, Chalk River, Ontario, Canada

S. Davies, Canadian General Electric Co., Ltd., 107 Park Street N., Petersborough, Ontario, Canada

Manager, Water Reactor Safety Program Office, Phillips Petroleum Co., Idaho Falls, Idaho 83401

J.J. Billington, Engineering & Physics, Dilworth, Secord, Meagher & Associates, 4195 Dundas St., West, Toronto, Ontario, Canada

J.D. Sainsbury, Atomic Energy of Canada, Ltd., Sheridan Park, Ontario, Canada

1 Atlantic Richfield Hanford Co., Richland, Washington

P.W. Smith

4 Atomic Energy Research Establishment, Harwell, England

A.E.J. Eggleton
W.J. Megaw
P. Goldsmith
R.A. Stinchcombe

1 Atomics International, Canoga Park, California

R. Kountz

1 Babcock & Wilcox Co., Lynchburg, Virginia

D.A. Nitti

3 Battelle Memorial Institute, Columbus, Ohio

J.M. Genco
J.A. Gieske
D.L. Morrison

1 Brookhaven National Laboratory

A.W. Castleman, Jr.

1 California Institute of Technology

S.K. Friedlander

1 Douglas-United Nuclear, Richland, Washington

T.W. Ambrose

1 du Pont, Savannah River Laboratory, Aiken, S. Carolina

A.H. Peters

2 General Atomics, San Diego, California

D. Busch
H.H. Van den Bergh

2 General Electric Co., APED, San Jose, California

H.V. Clukey
M. Siegler

1 Georgia Institute of Technology

C. Orr

1 Harvard University

F.J. Viles, Jr.

1 National Center for Atmospheric Research

R.D. Cadle

1 North Carolina State University

M.N. Ozisik

9 Oak Ridge National Laboratory, Oak Ridge, Tennessee

R.E. Adams
W.E. Browning, Jr.
W.B. Cottrell
M.H. Fontana
G.N. Keilholtz
L.F. Parsely, Jr.
G.W. Parker
T.H. Row
G.M. Watson

1 Oregon State University

J.G. Knudsen

1 Reactor Development Laboratory, Windscale, England

D.A. Collins

2 University of Minnesota

K.T. Whitby
B.Y. Liu

1 University of Pittsburgh

M. Corn

1 University of Texas

J.R. Brock

2 Westinghouse Electric Co., (APD)

W.D. Fletcher
J.D. McAdoo

61 Battelle-Northwest, Richland, Washington

J.M. Batch	C.L. Simpson
M.T. Dana	G.A. Sehmel
C.E. Elderkin	W.G.N. Slinn
J.J. Fuquay	E.C. Watson
J.M. Hales (20)	N.G. Wittenbrock
T.W. Horst	M.A. Wolf
B.M. Johnson	Technical Information (5)
J.D. McCormack	Technical Publications (1)
A.K. Postma	
G.J. Rogers	
L.C. Schwendiman (20)	